Quaternary Science Reviews 344 (2024) 109006

Contents lists available at ScienceDirect

Quaternary Science Reviews

journal homepage: www.elsevier.com/locate/quascirev

Sediment recycling during the Holocene marine transgression in Ría de Vigo (NW Iberia): multiproxy evidence and environmental implications

C. Muñoz Sobrino [a,b,*], A. Castro-Parada [a,b], V. Cartelle [c], N. Martínez-Carreño [d], C. Delgado [e], N. Cazás [a,b], I. Lázaro [a,f], S. García-Gil [a,f]

[a] Centro de Investigación Mariña, Universidad de Vigo, Vigo, Spain
[b] Dept. Bioloxía Vexetal e Ciencias do Solo, Universidade de Vigo, Facultade de Ciencias s/n E-36210, Vigo, Spain
[c] Flanders Marine Institute (VLIZ), InnovOcean Campus, Jacobsenstraat 1, 8400, Oostende, Belgium
[d] Centro Oceanográfico de Vigo Spanish Institute of Oceanography (IEO-CSIC), 36390, Vigo, Spain
[e] Departamento de Ecoloxía e Bioloxía Animal, Universidade de Vigo, Facultade de Ciencias s/n E-36210, Spain
[f] Dept. Xeociencias Mariñas, Universidade de Vigo, Facultade de Ciencias s/n, E-36210, Vigo, Spain

ARTICLE INFO

Handling editor: Giovanni Zanchetta

Keywords:
High system tract
Sea level
Postglacial
Coastal wetlands
Coastal hydrology
Pinewoods
Reworked pollen

ABSTRACT

A new multiproxy study of a 155-cm sediment core located in Ría de Vigo (NW Iberia) recording the transgressive and highstand system tract of the Holocene sea-level rise is presented. New data described include grain size, geochemical analyses, high-resolution qualitative/quantitative analyses of pollen, non-pollen palynomorphs and dinoflagellate cysts content, the qualitative evaluation of diatoms at different key levels and the reconsideration of some seismic interpretations. Besides, 14 radiocarbon dates were obtained from shells and pollen extracts. This new evidence revealed that notable changes in the sedimentation rates and the relative abundance of the different types of palynomorphs occurred during the Holocene. The sediment core studied shows anomalous pollen successions, including unexpected *Pinus* pollen peaks, during the Early and Middle-Holocene. Differential dating revealed that those anomalous successions correspond to conspicuously aged sediment that has inverted pollen chronologies. Thus, these facies may constitute evidence of redeposition of ancient upland sediments, formed above the ancient coastline at different intervals comprised between the end of the Last Glacial Maximum and the early stages of the Lateglacial, which were rich in very resistant pollen types (*Pinus*). Dinoflagellate cyst records in combination with the non-reworked pollen evidence reveal a reliable climatic seesaw during the Holocene, includingwet stormy periods of prevailing mixed waters, with strong development of *Lingulodinium* and high accumulation rates in dinoflagellate cysts, which alternate with other sparsely stormy and drier phases, characterised by the coastal upwelling intensification, well-stratified waters, and increases in *Bitectatodinium* and *Spiniferites* spp. but low accumulation rates in dinoflagellate cysts. These climatic dynamics, including a millennial drier cool period that occurred just after the Thermal Optimum are consistent with previous evidence obtained in other limnetic systems in the Iberian Peninsula. Furthermore, there is a delay between the two phases with the highest marine contribution to sediment (ca. 11.0-8.2 and ca. 4.0–3.0 cal ka BP) and the subsequent warm stages when the relative sea level stabilises: the Thermal Optimum (8.0–6.0 ka BP) and the 2.5-0.5 ka BP interval, respectively. Changes in *Pinus* pollen concentrations and grain size recorded in the postglacial sediments suggest that some upland ancient (Lateglacial) pollen evidence might be remobilised, especially during stages of upwelling intensification, and then resedimented in the seabed. Further studies will be needed to determine if the significant differences existing between the *Pinus* pollen grain sizes respond to climatic variations affecting the region or have been the result of any replacement of pine species in the area. Nonetheless, *Pinus* pollen evidence almost disappeared with the first signs of anthropisation in the area, and only recovered after the modern repopulations. Our findings open up new possibilities to further our understanding of sediment reworking and recycling mechanisms through the integration of multiproxy studies encompassing pollen, seismic and sedimentary data.

* Corresponding author. Centro de Investigación Mariña, Universidad de Vigo, Vigo, Spain.
E-mail address: bvcastor@uvigo.es (C. Muñoz Sobrino).

https://doi.org/10.1016/j.quascirev.2024.109006
Received 24 May 2024; Received in revised form 13 September 2024; Accepted 11 October 2024
Available online 17 October 2024

1. Introduction

Palynomorphs can be found in almost all sedimentary systems and, therefore, they are of great value to directly date pollen stratigraphic boundaries and to understand ancient environmental conditions. Particularly, the study of microremains in fluviomarine sediments is a common method for simultaneously studying marine and terrestrial realms over time. Some of the key paleoenvironmental parameters reconstructed using these methods include changes in freshwater inputs, sea-land climatic interactions, and marine productivity patterns (e.g., de Vernal, 2009; Muñoz Sobrino et al., 2012; Donders et al., 2018; García-Moreiras et al., 2018; Mudie et al., 2021; Yedema et al., 2023). Moreover, the study of marine and terrestrial palynomorphs in fluviomarine environments has been successfully used in combination with different geophysical approaches to understand high-resolution relative sea-level oscillations and to reconstruct the environmental changes affecting estuaries and other nearby inland ecosystems (Muñoz Sobrino et al., 2014; 2018, 2022; García-Moreiras et al., 2019a; Cartelle et al., 2022).

The availability of useful chronologies is also crucial for paleoenvironmental reconstructions. During the last decades, the Accelerator Mass Spectrometry (AMS) radiocarbon measurement of terrestrial or marine macrofossils became the most common technique for building robust age models in sedimentary contexts younger than 40 000–45 000 years old (e.g. Björk and Wohlfarth, 2001). Macrofossils may be sparse or irregularly present, while pollen has the advantage of being present in many different types of sediments and throughout a whole sequence. Thus, in the absence of sufficient macrofossils, pollen concentrates may represent a valuable source of dates if the sediment has enough pollen content for a radiocarbon date and can be effectively isolated from other carbon-bearing material (Tunno et al., 2021). Marine sediments are frequently poor in pollen content, but estuarine and fluviomarine sediments are notable exceptions. Maximum deposition in those environments can take place at some distance from the shore, presumably when the diameter (4–16 μm) and sinking rate of the mineral grains correspond to those of the pollen grains (Faegri et al., 1989). Another intrinsic advantage of dating pollen from fluviomarine systems is that it is predominantly of terrestrial origin and not influenced by reservoir effects.

A significant disadvantage of dating pollen at different levels may be the differential preservation of pollen over time, depending on the changing taphonomic conditions (e.g. Keil et al., 2014), but also the intrinsic characteristics of each palynomorph. Hopkins and McCarthy (2002) found that pollen was more resistant to oxidation than dinoflagellate cysts and that bisaccate conifer pollen was the most resistant of all forms studied. In general, the propensity of pollen to be preserved in sediments depends largely on the amount of sporopollenin in the exine, which is a function of the thickness of the exine and the proportions of its components (the more ektexine, the more sporopollenin). *Pinus* pollen is abundantly produced, relatively buoyant (e.g., Castro-Parada and Muñoz Sobrino, 2022), and rich in sporopollenin (Traverse, 2008). Therefore, it is not surprising that bisaccate pollen, particularly that of *Pinus*, is frequently overrepresented in past (e.g., Sánchez-Goñi et al., 2018) and modern (e.g., Dai et al., 2014; Luo et al., 2014; García-Moreiras et al., 2015, 2023; Yedema et al., 2023) marine and fluviomarine sediments.

Another consideration when dating pollen is the problem of anomalous pollen deposition, including secondary, recycled and rebedded pollen, phenomena that can affect both continental and marine sediments (e.g., Stanley, 1966; Streel and Bless, 1980; Li et al., 2012; Krüger and Damrath, 2020). Marine environments largely include evidence of reworked sporomorph grains over longer non-successive geological timescales easily identifiable within younger sporomorph assemblages. Nevertheless, distinguishing non-reworked from reworked material in palynological assemblages over successive geological periods may be more problematic (Strother et al., 2017).

During the last decades several multiproxy studies performed in fluviomarine systems from NW Iberia (Fig. 1A) have described different Holocene (e.g. Desprat et al., 2003; Muñoz Sobrino et al., 2007; 2012, 2014, 2016, 2022; García-Moreiras et al., 2018) and Pleistocene (e.g. García-Moreiras et al., 2019a) periods but no complete transgressive sequence has been studied in detail so far. This study presents new multiproxy analyses of the Holocene section of a sediment core located in Ría de Vigo (Fig. 1AB). According to previous seismic stratigraphic studies (Fig. 1C) the new levels studied (0–155 cm) include the transgressive and highstand system tracts corresponding to the sea-level rise following the Last Glacial Maximum (Martínez-Carreño and García-Gil, 2017). New evidence presented here includes grain size and geochemical analyses, high-resolution qualitative and quantitative analyses of the pollen, non-pollen palynomorphs (NPP) and dinoflagellate cysts content, a qualitative evaluation of the diatoms content at different key levels, and differential dating of shells and pollen samples along the transgressive sequence. The main objective is to perform a detailed environmental reconstruction during the Holocene transgression to evaluate the main factors driving the processes of sedimentation, including climate, sea level, coastal hydrology and human impact, aiming at providing insight into the complexity of these sedimentary systems and the processes of short-term sediment recycling.

2. Study area

Galician rias are located on the eastern passive Atlantic margin of Galicia (NW Iberia) and comprise the *Rías Altas* to the north of Cape Finisterre and the *Rías Baixas* to the south (Fig. 1A). The rias are non-glaciated submerged incised valleys, and their sedimentary infill is generally the result of multiple cycles of incision and deposition (Martínez-Carreño and García-Gil, 2017; Cartelle and García-Gil, 2019; Cartelle et al., 2022). The *Rías Baixas* include the southernmost of all the Galician rias, the Ría de Vigo (RdV, Fig. 1A).

Ría de Vigo (175 km^2) has a funnel shape in plan view, with the Cíes Islands partially blocking its connection to the open sea, and the Rande Strait (a narrow channel 600 m across and 1.5 km long) connecting the outer ria with the San Simón Bay (Fig. 1A). The flooded valley extends more than 35 km in length and less than 15 km in width, and the total catchment of the basin comprises about 709 km^2 (Pérez-Arlucea et al., 2000). The water depth varies between <7 m in San Simón Bay to 53 m in the southern outer ria. It corresponds to a mesotidal coast, with an average tidal range of 2.2 m and a semi-diurnal cycle. A marked horizontal salinity gradient exists from the inner part of the ria (~31–32 psu), where the main rivers in the area flow (Verdugo-Oitavén and Alvedosa), towards the outer part (36 psu = practical salinity unit). Sea surface temperature (SST) is ~15 °C on average, varying between 19 and 20 °C during summer and 11–12 °C during winter (Pérez-Arlucea et al., 2007).

The Galician margin is characterised by a narrow continental shelf (ca. 30 km) with the shelf break at c. −150 m relative to present-day sea level (Fernández-Salas et al., 2015). Thus, the rias are semi-closed bays that behave like an extension of the shelf rather than typical well-mixed estuaries, with weakly stratified waters generally dominating throughout the year (Villacieros-Robineau et al., 2013). The Atlantic coast of NW Iberia (Fig. 1A) is in the eastern margin of the mid-latitude Atlantic Ocean, and thus affected by the northern boundary of the Canary Current upwelling system and influenced by the Eastern North Atlantic Central Water (ENACW). Seasonal upwelling intensifying the thermal stratification of coastal waters in summer is promoted by the latitudinal shift of the Azores-High/Icelandic-Low pressure system (Rodríguez et al., 2023) so that the Portugal Current System (PCS) dominates the surface offshore western Iberian by flowing towards the Equator in summer and towards the Arctic in winter (Otero et al., 2008). Two branches of the ENACW flow under the PCS: the subtropical water (ENACWst) and the subpolar water (ENACWsp).

Currently, the main synoptic weather types in the region result from a combination of the North Hemisphere Annular Mode (NAM) and other

large-scale atmospheric modes, namely the North Atlantic Oscillation (NAO), the Scandinavian Pattern (SCA), the Eastern Atlantic (EA), and the Eastern Atlantic/Western Russia (EA/WR). Therefore, most annual rainfall can be explained by cyclonic, western, and south-western weather types that prevail when the NAO index stays negative. Alternatively, a positive NAO index reduces the occurrence of cyclonic weather in winter, but the EA mode has a positive annual correlation with W and SW weather types that produce increasing rainfall in spring, summer, and autumn (Lorenzo et al., 2008). Weather seasonality drives the oceanic conditions on the Galician coasts because the predominance of northeasterly winds during spring-summer promotes upwelling of cold, salty and nutrient-rich water (ENACW) on the shelf, but the predominance of south-westerly winds during autumn-winter promotes downwelling and modifies the development and composition of phytoplankton populations in the Galician Rías (Nogueira et al., 2022; Rodríguez et al., 2023).

The southern margin of RdV has the highest population density in the area (Fig. 2A), but the rest of the basin is only moderately populated, and consists of a complex mosaic of urban soil, forest plantations (mainly *Eucalyptus* spp. and *Pinus* spp.), shrubs (*Erica* spp., *Calluna vulgaris* (L.) Hull., *Ulex* spp., *Cytisus* spp., *Cistus* spp.) and sparse stands of deciduous oak forests with *Quercus robur* L., riparian woodlands (mainly formed by *Alnus lusitanica* Vít, Douda & Mandák, *Corylus avellana* L., *Fraxinus angustifolia* Vahl. and *Salix* spp.) and evergreen laurel forests (*Laurus nobilis* L., *Ilex aquifolium* L.). Fluviomarine transitional areas encompass diverse habitats related to marshes, sandy intertidal flats, estuarine-deltaic complexes, beaches, and muddy intertidal flats (Ramil-Rego et al., 2008).

3. Materials and methods

The MVR-3 vibracore was recovered on board the research vessel RV *Mytilus* in July 2012 at a water depth of - 30 m in the outer part of RdV (Fig. 1A). Martínez-Carreño and García-Gil (2017) provided a detailed lithostratigraphic study of the complete core and an interpretation of its seismic stratigraphic context. The total length of the core is 279 cm, and the deepest section (155–279 cm) corresponds to Upper Pleistocene. This section was analysed and discussed in Muñoz Sobrino et al. (2018) and García-Moreiras et al. (2019a), including a few samples from the overlying sediments corresponding to the Early Holocene. All pollen

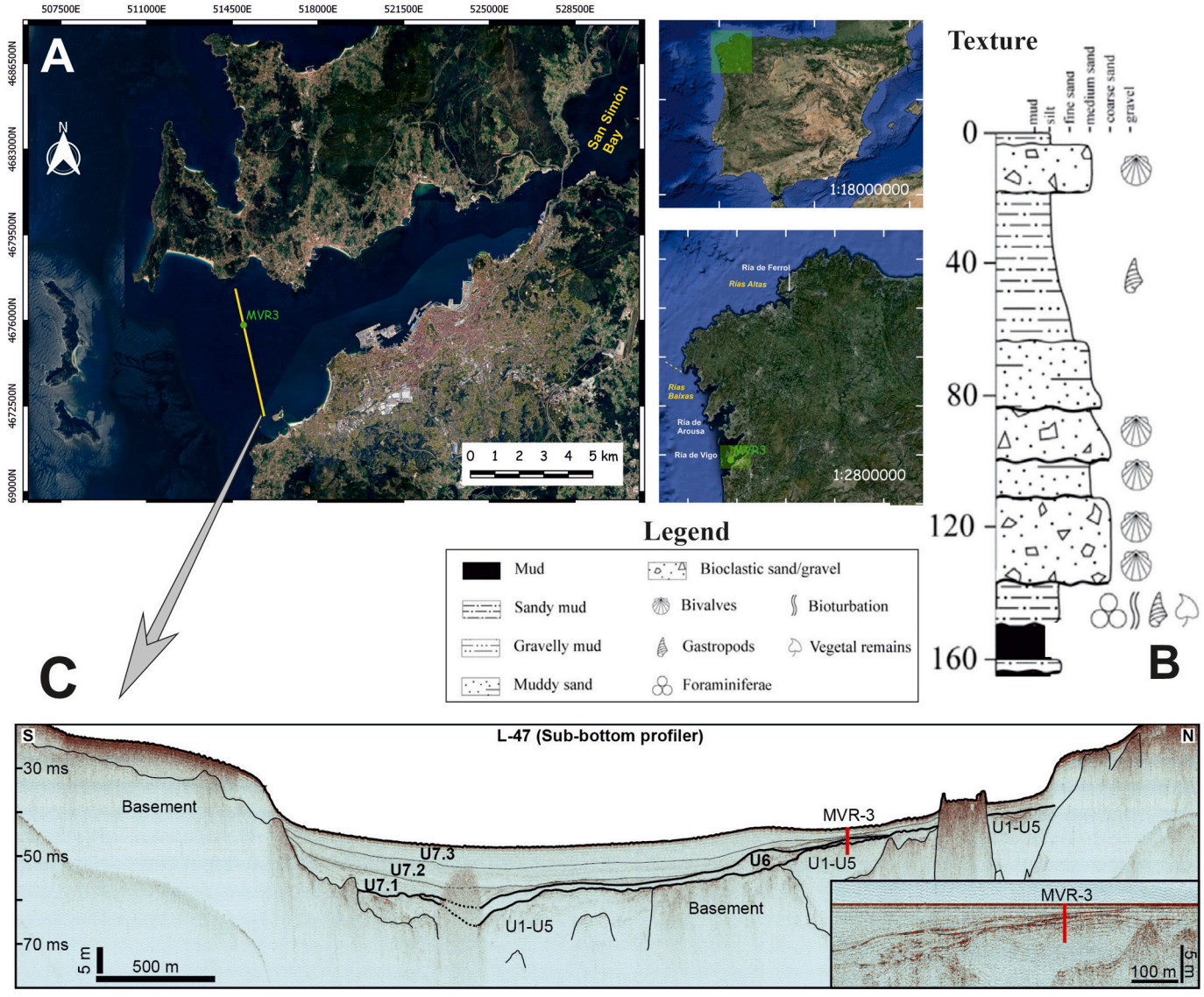

Fig. 1. A) Location map. B) Lithology of the upper 155 cm of core MVR-3, Ría de Vigo, NW Iberia. C) High-resolution seismic profile (3.5 kHz) across the study site showing the location of core MVR-3 and the seismic stratigraphic interpretation. The zoomed-in inset (flattened using the seabed) illustrates the complexity of seismic units U6 and U7 at the location of MVR-3.

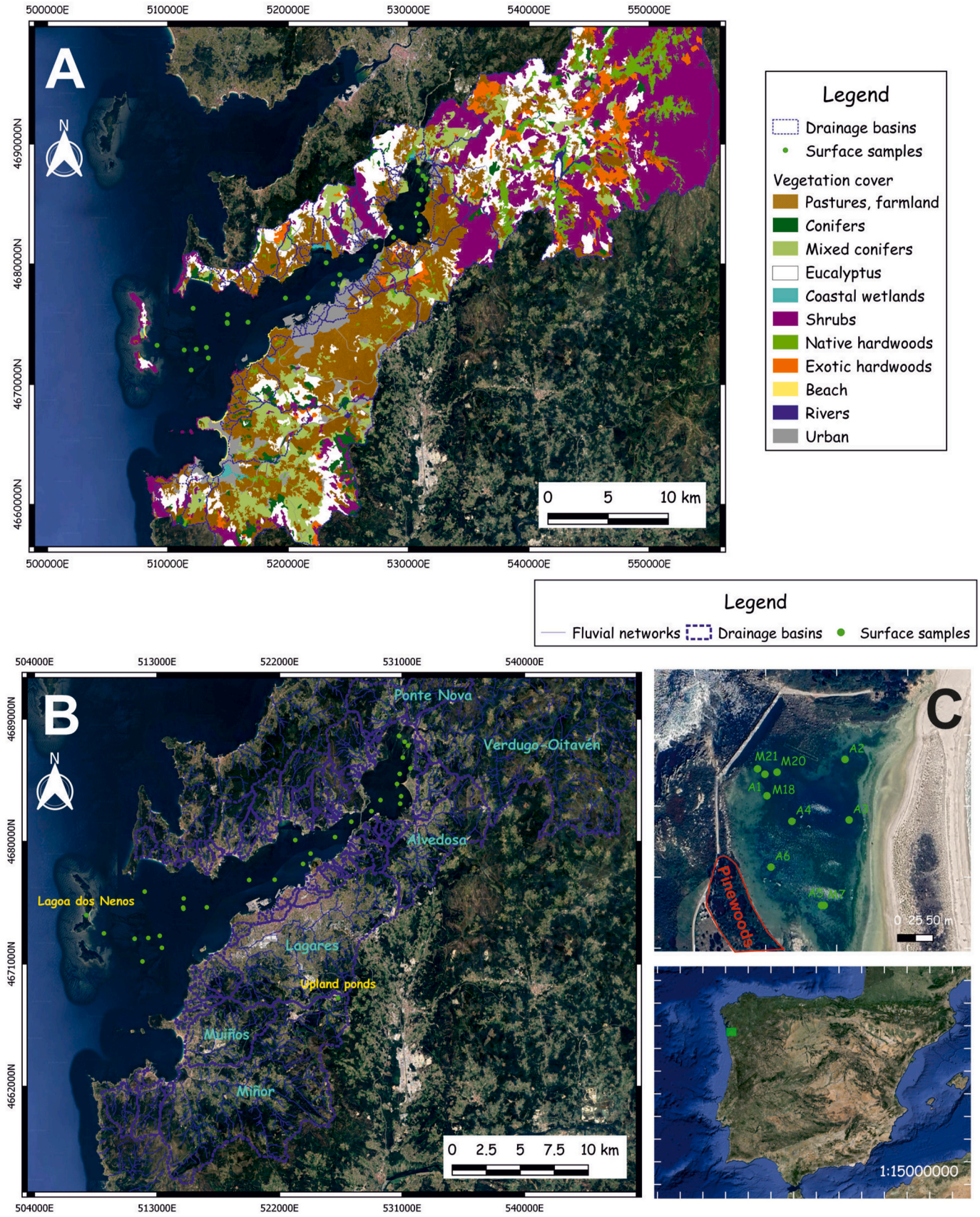

Fig. 2. A) Image analysis of the modern vegetation cover in the Ría de Vigo basin. Location of the modern pollen samples studied in: B) modern seabed (Castro-Parada et al., 2023) and upland ponds (Castro-Parada and Muñoz Sobrino, 2022), and C) Lagoa dos Nenos (Muñoz Sobrino et al., 2016).

samples presented here (0–155 cm) were analysed again to homogenise all the taxa identified and to incorporate some key palynomorphs (cf. *Juncus;* Muñoz Sobrino et al., 2022) that were not formerly recognised. This study includes a new interpretation of the palaeoenvironmental changes that occurred in the area during the Late glacial and the Holocene, which is based on the combination of high-resolution seismic records with other centennial-to-millennial multi-proxy analyses. The latter include geochemistry and the analysis of pollen, dinoflagellate cysts and diatom content. Parallel, a robust Holocene chronology was performed based on macro and microremains extracted from the MVR-3 vibracore.

3.1. Geophysical data

Seismic data in the Ría de Vigo was acquired using a modified boomer system consisting of a single boomer source (AAE CSP 300, 1.5 kHz) and two receivers, a single-channel streamer (AAE 8 & 20) and a sub-bottom profiler (3.5 kHz). A total of 795 km of seismic profiles were recorded onboard the RV *Mytilus* as part of several projects. A differential positioning system was used for navigation and positioning (Trimble Inc. AgGPS 132 receiver). The stratigraphic interpretation of these profiles was carried out by Martínez-Carreño and García-Gil (2017), who identified up to seven distinct seismic units (U1 to U7), of which U2 to U5 were attributed to the Pleistocene, U6 to the Upper Pleistocene to Holocene transition and U7 mainly to the Holocene.

3.2. Grain size and geochemical analyses

The grain size distribution of the MVR-3 core was determined at 5–20 cm intervals, depending on the visual inspection of the lithology (Fig. 1B). Organic matter of each sample was removed using hydrogen peroxide and the clay fraction was dispersed by adding sodium hexametaphosphate. Large fragments of shells were excluded to avoid data biasing, and the suspension was then sieved to separate the different fractions. The sandy fraction was determined by a standard dry-sieving procedure after drying at 60 °C. The distribution of clay and silt was determined using a Micromeritics SediGraph 5100. Total Nitrogen (TN) and Total Inorganic Carbon (TIC) content were determined at the same intervals by combustion with a Carlo Erba-EA1108 elemental analyser. Total Organic Carbon (TOC) was analysed using a ThermoFinnigan FlashEA 1112 analyser after acidification with 30% HCl. N and C values are expressed as percentages of dry weight (wt%) (Table S1).

3.3. Chronology

Radiocarbon dating was performed by the Beta Analytic Laboratory in Miami (Florida, USA) using AMS standard dating methods. Fourteen radiometric dates corresponding to the MVR-3 core (Table 1) were obtained from shells (3) and pollen extracted from sediment at different depths (11) to try to date several major changes in the pollen record. Dates on marine samples were calibrated using the MARINE20.14C calibration curve (Stuiver et al., 2020) and applying a local marine reservoir correction of $\Delta R = 12 \pm 163$ (Reimer and Reimer, 2001) that corresponds to the average of the nearest ten points in Stuiver et al. (2020). Pollen remains for dating (Brown et al., 1992; Li et al., 2012) were extracted after applying several successive KOH treatments and sieving (<250 μm - >10 μm) to remove the unsaturated organic colloids (Faegri et al., 1989) and other sources of organic carbon. $\delta^{13}C$ values obtained (Table 1) confirm that most of the organic matter of marine origin in these samples was removed by the sample treatment (Lamb et al., 2006; Lee et al., 2020). Pollen samples were calibrated by using the INTCAL20.14C calibration curve (Stuiver et al., 2020). The software BACON 2.3.9.1 (Blaauw and Christen, 2011) was used to produce the age-depth model (Fig. 3). Dates selected or rejected to perform a consistent age-depth model are indicated in Table 1 and Fig. 3. Nevertheless, all the dates obtained, including those aged or inverted, have been useful in building a coherent model of sedimentation that eventually includes the reworking of ancient, emerged sediments; and therefore, they were also valuable in the discussion and interpretation of the sequence. Finally, some of the pollen benchmarks (correlated to historical evidence) previously adopted by Muñoz et al. (2014) were also used to refine the chronologies corresponding to the last centuries (Table 2; Fig. 3).

3.4. Pollen, dinoflagellate cysts and NPP

New pollen, dinoflagellate cysts and non-pollen palynomorphs (NPP) analyses were performed for the upper 155 cm of the MVR-3 core. 66 subsamples of 1.5–5.5 cm^3 of fresh sediment were taken at variable (1–5 cm) intervals and processed using standard methods (Faegri et al., 1989; Mertens et al., 2009). Thus, samples were dried (80 °C), spiked with *Lycopodium* spores for concentration and accumulation rate estimates, treated with HCl and HF (room temperature), and sieved to remove coarse (>250 μm) and fine (<10 μm) materials.

Palynomorphs were identified and counted using a light microscope (LM) Nikon Eclipse 50i at 400 × and 600 × magnifications. The total pollen sum identified in each sample was reliable in all the cases (ranging between 186 and 626, 291 on average), but the total dinoflagellate cyst identified notably varies along the core (ranging between 17 and 260, 84 on average). The identification and nomenclature of pollen types are mainly based on Moore et al. (1991). Terrestrial pollen percentages were calculated upon a terrestrial pollen sum, but the percentages of aquatics (freshwater taxa and bryophytes) are based on the total pollen sum. To simplify the text, several freshwater-related taxa (e.g., *Ranunculus*-type, Cyperaceae, *Isoetes*, cf. *Juncus*) are grouped and commonly designed as aquatics, but we assume that some species included in these groups may be indistinctly hydrophytes, helophytes or simply developing on wet soils. The taxon cf. *Juncus* corresponds to the palynomorph described in Muñoz Sobrino et al. (2022). The percentages of the different types of dinoflagellate cysts (identified groups follow Zonneveld et al., 2013) were calculated in relation to the total dinoflagellate cysts count. Non-pollen palynomorph (NPP) percentages, including mainly microforaminiferal linings (Stancliffe, 2002) and fungal and fresh/brackish-water algae remain (van Geel et al., 1989; van Geel, 2003), were based on total pollen plus NPP. The ratio of dinoflagellate cyst concentrations to pollen, fern spores and dinoflagellate cyst concentrations (D/P ratio, ranging between 0 and 1; modified as the inversed ratio used by McCarthy and Mudie, 1998) was calculated for each sample to show the temporal variation. Besides, H/A index, i.e., the ratio of heterotrophic cysts to total cysts (heterotrophic + autotrophic cysts) was also calculated for all the samples.

3.5. Numerical analyses

TILIA 2.6.1 software (Grimm, 1990–2019) was used to process the data and produce the diagrams (Fig. 4). The pollen record was zoned using a constrained incremental sum of squares (CONISS) cluster analysis with Euclidian distance (Fig. 4). Anomalous pollen successions are reported below, including unexpected *Pinus* pollen peaks during the Early and Mid-Holocene that have not been previously described in the area (Gomez-Orellana et al., 1998; Kaal et al., 2011; Muñoz Sobrino et al., 2012; García-Moreiras et al., 2019a). To try to estimate the rebedded pollen contribution, the average of dark pollen (mainly specimens of *Pinus* subgenus *Pinus* and *Erica* in variable proportions) was calculated (Table S2) for each Local Pollen Assemblage Zone (LPAZ). This proportion was subtracted from the *Pinus* subgenus *Pinus* raw data to recalculate the percentages of the main pollen types (Fig. 4). CONISS results after discarding the proportion of the estimated rebedded pollen are consistent with the LPAZ obtained using the original raw data (Fig. 4).

For the discussion of the results, the pollen concentrations in the MVR-3 core were compared with those of the modern data obtained by

Table 1
Radiocarbon dates available and included (*) in the age-model. Modern ages also used in Fig. 2 correspond to pollen inferences in Table 2.

LAB0RATORY CODE	Depth (cm)	AMS Radiocarbon Age	IRMS $\delta^{13}C$ (‰)	1-Sigma cal yr BP	Probability	2-Sigma cal yr BP	Probability	Median Probability Age (cal yr BP)	Material	Calibration Curve	Comments	Nº in Fig. 3
Beta – 632630	30–31	2100 ± 30	−6.9	2003–2027	0.282	1952–1956	0.007	*2062*	Pollen (extracted)	**INTCAL20**	**REWORKED**	**5**
				2040–2105	0.718	1992–2146	0.985					
						2279–2285	0.007					
Beta – 590785	44–45	2170 ± 30	−4.4	2116–2157	0.422	2052–2183	0.509	2179 (*)	Pollen (extracted)	**INTCAL20**	**AGE MODEL**	**6**
				2171–2175	0.018	2192–2212	0.032					
				2239–2300	0.561	2223–2308	0.459					
Beta – 632631	54–55	2880 ± 30	−8.0	2960–3009	0.526	2882–2905	0.035	3008 (*)	Pollen (extracted)	**INTCAL20**	**AGE MODEL**	**7**
				3011–3060	0.474	2921–3078	0.899					
						3093–3110	0.028					
						3122–3145	0.037					
Beta – 590786	65–66	4860 ± 30	−9.4	5492–5500	0.090	5482–5514	0.164	*5592*	Pollen (extracted)	**INTCAL20**	**REWORKED**	**8**
				5581–5602	0.824	5517–5526	0.015					
				5639–5646	0.086	5575–5608	0.635					
						5621–5656	0.186					
Beta – 590787	75–76	16620 ± 50	−13.3	19983–20175	1.000	19909–20252	1.000	*20084*	Pollen (extracted)	**INTCAL20**	**REWORKED**	**9**
Beta – 632632	90–91	15250 ± 40	−13.2	18333–18462	0.796	18295–18505	0.718	*18432*	Pollen (extracted)	**INTCAL20**	**REWORKED**	**10**
				18629–18668	0.204	18588–18701	0.282					
Beta-325297	94–96	5700 ± 30	−2.4	5699–6095	1.000	5525–6272	1.000	5890 (*)	Shell	**MARINE20**	**AGE MODEL**	**11**
Beta – 590788	105–106	5180 ± 30	−7.7	5911–5940	0.664	5901–5996	1.000	5938 (*)	Pollen (extracted)	**INTCAL20**	**AGE MODEL**	**12**
				5970–5987	0.336							
Beta – 632633	109–110	6890 ± 30	−8.7	7677–7743	1.000	7665–7791	0.993	7718 (*)	Pollen (extracted)	**INTCAL20**	**AGE MODEL**	**13**
						7818–7823	0.007					
Beta – 590789	124–125	13600 ± 40	−10.8	16336–16495	1.000	16278–16580	1.000	*16420*	Pollen (extracted)	**INTCAL20**	**REWORKED**	**14**
Beta – 632634	130–131	12970 ± 40	−9.6	15430–15618	1.000	15324–15669	1.000	*15519*	Pollen (extracted)	**INTCAL20**	**REWORKED**	**15**
Beta – 320481	138	9830 ± 50	+1.4	10343–10871	1.000	10177–11119	1.000	10624 (*)	Shell	**MARINE20**	**AGE MODEL**	**16**
Beta – 632635	140–141	18170 ± 50	−8.5	22060–22197	1.000	21997–22271	1.000	*22131*	Pollen (extracted)	**INTCAL20**	**REWORKED**	**17**
Beta – 411503	146–147	10370 ± 40	−0.1	11145–11638	1.000	10867–11916	1.000	11387 (*)	Shell	**MARINE20**	**AGE MODEL**	**18**

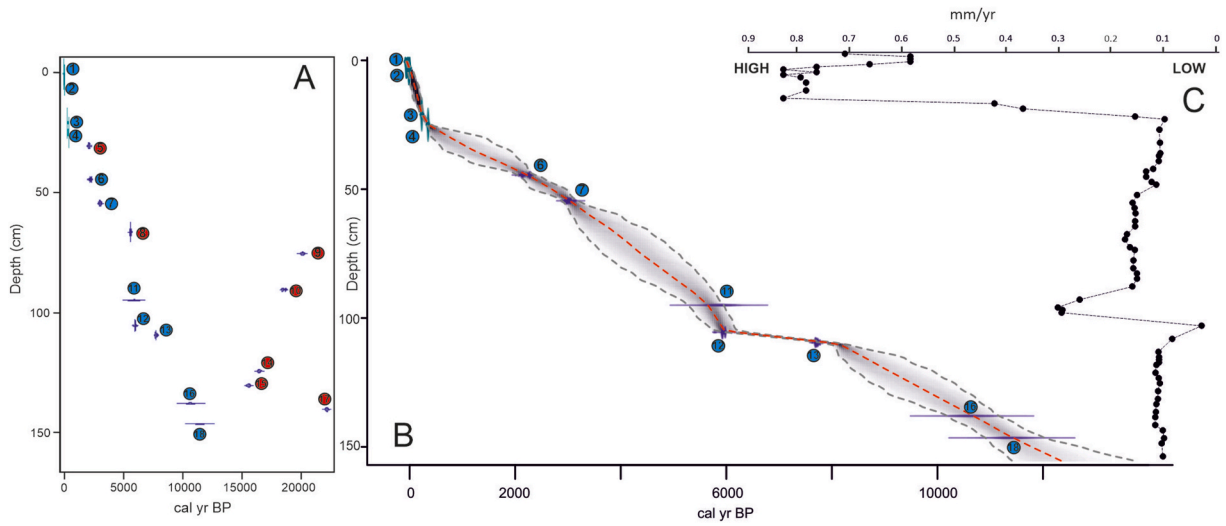

Fig. 3. A) Radiocarbon dates available (in blue, dates selected for the age-depth model and outliers in red); B) Age model produced using pollen benchmarks (turquoise) and selected radiocarbon dates (blue), and C) accumulation rates estimated using the age-depth model produced. For details of dates and age-depth modelling, see Table 1, Table 2, and discussion in the text.

Table 2
Historical events described in the literature that may be supported by the environmental reconstruction resulting from the analyses performed in core MVR-3.

Nº pollen event in Fig. 4	Age AD	Age cal. a BP	MVR-3 Depth (cm)	Pollen event	References
1	2010	−60	1		Data of coring (rounded)
2	1960	−10	3	Extensive reforestation with *Eucalyptus*	Ramil-Rego et al. (2012)
3	1720	230	21	Regional reintroduction of pinewoods	Bouhier (2001)/^{14}C in Muñoz Sobrino et al. (2007)
4	1600	350	25	Early introduction of *Zea mays* L.	Vazquez et al. (2007)

Castro-Parada and Muñoz Sobrino (2022) and Castro-Parada et al. (2023) in the same basin (Fig. 2). Finally, a biometric study of the *Pinus* subgenus *Pinus* pollen evidence was performed following Desprat et al. (2015) to evaluate discriminating the modern repopulations with *Pinus pinaster* Aiton from the previous *Pinus* pollen evidence. Therefore, the total grain sizes of a representative number of specimens (ranging between 37 and 75, taken in more than three samples from each pollen zone), were studied. Summary statistics, normality tests, and hierarchical cluster analysis were performed to analyse the similitudes of the *Pinus* pollen sizes between different pollen zones. To determine whether differences in *Pinus* pollen sizes observed between pollen zones were significant, Turkey's, Mann-Whitney, and Dunn's post hoc pairwise tests were applied to subsamples taken for each LPAZ. Descriptive statistics and other multiple-sample tests (Tables S3, S4, S5, S6) were performed using the PAST software (Hammer et al., 2001). Boxplots for concentrations of selected pollen types and total grain sizes per LPAZ were created using Microsoft Excel.

3.6. Diatoms

Diatom content was also studied in 17 samples taken in 1-cm sections all along the upper 155 cm of the MVR-3 core. Approximately 0.2–0.3 g of sediment was collected per sample, dried, and prepared by standard procedures. Each sample was cleaned with 4–6 cm^3 of 65% HNO_3 and potassium dichromate ($K_2Cr_2O_7$) at room temperature for 24–48 h and added few drops of HCl. Later, the samples were repeatedly centrifuged (1500 rpm) and rinsed with distilled water to remove oxidation by-products. Finally, permanent slides were mounted using Naphrax® mounting resin with high refractive index (1.65). Two slides (22 × 22 mm) of each sample were examined for diatom content using a Nikon Eclipse E800 light microscope (LM), equipped with an immersion objective 100× (NA 1.40) to assess the relative abundance of taxa. Light micrographs were captured with DS-U2 digital camera and NIS-Elements D 2.30 SP1 software (Nikon, Japan, Plate 1). Diatoms were identified to the lowest taxonomical level mainly according to Krammer and Lange-Bertalot (1991, 1999a, 1999b, 2000), Lange-Bertalot (1993, 2001), Hasle and Syvertsen (1996), Witkowski et al. (2000), Levkov et al. (2010) and Trobajo et al. (2013).

4. Results

4.1. Seismic stratigraphy

The section of the vibracore MVR-3 of interest for the present work (0–155 cm) corresponds to the two shallowest and youngest seismic units (U6-U7) of Ría de Vigo following the stratigraphic interpretation of Martinez-Carreño and García-Gil (2017). Seismic unit 6 (U6) appears scattered along the basin of the ria, generally thin (<5m) but reaching up to 11 m in the axis of the valley and the outermost parts. This unit is onlapping an erosive surface at its base and another disconformity erodes its top. Towards the basin margins, the seismic facies of U6 are characterised by parallel subhorizontal continuous reflections displaying multiple phases of vertical aggradation with onlap terminations (Fig. 1C). Seismic unit 7 (U7) corresponds to the youngest sedimentary infill of the ria, being its top boundary the present-day seabed (Fig. 1C). U7 is the most widespread and continuous unit in the ria. The seismic facies of U7 generally correspond to parallel subhorizontal continuous reflections with onlap terminations, but locally displaying progradation and downlaping reflections. A new interpretation has allowed us to further distinguish three seismic subunits within U7 (U7.1 to U7.3), bounded by minor discontinuities that denote changes in the sedimentary patterns in the ria. Seismic sub-unit 7.1 is the less extensive and is absent in the inner part of San Simón Bay. It thins towards the edge of the ria, except in those areas where prograding sedimentary bodies are developed. Sub-unit 7.2 is laterally more extensive, draping the underlying deposits. At the site where MVR-3 was collected sub-units 7.1 and

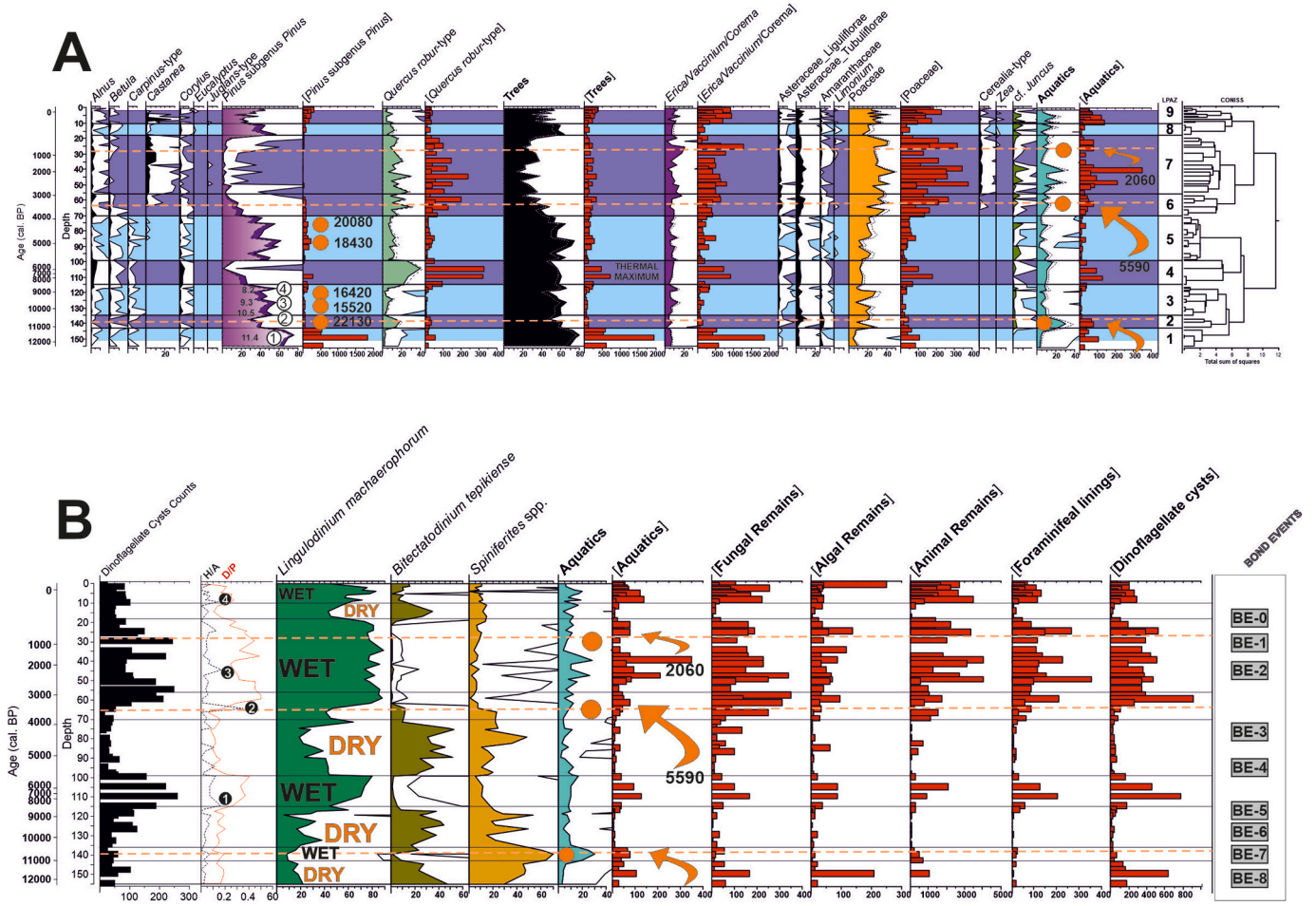

Fig. 4. Summarised pollen analyses of the upper 155 cm of core MVR-3, Ría de Vigo, NW Iberia, including (A) percentages and concentrations [grains/cm^3] of the main pollen. The purple stripes represent the phases of greater precipitation and predominance of mixed waters, and the light blue stripes phases of increasing upwelling identified in B. Anomalous radiocarbon dates indicated as orange circles (see the text). Dotted orange lines represent those three rainy erosive events (note the low total tree pollen percentages) when upland ancient material was remobilised and resedimented in the seabed. The secondary curves of percentages (dotted) represent the values recalculated after discarding the rebedded pollen underestimated (see the text) in each LPAZ (Table 2); and (B) percentages and concentrations [grains/cm^3] of the main dinoflagellate cyst types, concentrations [grains/cm^3] of other NPPs, and Bond Events (BE). 1 to 4 in (A) indicates peaks of *Pinus* that are respectively interpreted as the Younger Dryas/11.4 ka transition (BE-8), 10.5 (BE-7), 9.3 (BE-6) and 9.2 ka (BE-5). 1 to 4 in (B) indicates the four peaks of H/A discussed in the text.

7.2 are thin condensed deposits and are difficult to distinguish due to the limit in the resolution of the seismic system. Sub-unit 7.3 is the most expansive and continuous in the ria and is characterised by a shift from predominantly aggrading deposits to extensive progradation in the basin margins.

4.1.1. MVR-3 chronology and accumulation rates (0–155 cm)

The age-depth model finally adopted for the upper 155 cm of core MVR-3 (Fig. 3) was built by using seven radiocarbon dates, three corresponding to macroremains (shells) and four pollen extracted from sediments (Table 1). Three radiocarbon dates (dates 5, 8 and 17; Table 1; Fig. 3) obtained from extracted pollen are outliers, probably upland ancient material that remobilised during rainy periods and resedimented in the seabed (Fig. 3). Another four radiocarbon dates upon pollen extracted from sediment (dates 9, 10, 14 and 15; Table 1; Fig. 3) resulted as apparently inverted in the sequence and notably aged. Thus, these samples were considered outliers and excluded from the age-depth model. Besides, another three pollen benchmarks were used to improve the chronology of the historical period, which respectively correspond to the regional introduction of corn (*Zea mays* L.), and the modern repopulations with pines and *Eucalyptus* (Table 2; Fig. 3). All three were consistently used in previous reconstructions in the area (e.g. Muñoz Sobrino et al., 2007, 2012, 2014). Other older pollen benchmarks related to the cultivation of *Castanea* were not used here for independently contrasting the new MVR-3 data with the chestnut dynamics previously described for this region (Desprat et al., 2003; Muñoz Sobrino et al., 2014; Gómez-Orellana et al., 2021). Applying this model, the complete sequence studied (0–155 cm) approximately records the last 12 200 cal a BP (Fig. 3). The new evidence presented revealed notable changes in the sedimentation rates (Fig. 3) during the Holocene (Fig. 5). Low accumulation rates occurred between 110 and 155 cm depth (ca. 0.1 mm yr^{-1}) that subsequently decay until minimum values recorded at 100–110 cm (ca. 0.02 mm yr^{-1}). Later, they notably increase between 100 and 90 cm (0.3 mm yr^{-1}) and stabilize at ca. 1.5 mm yr^{-1} between 90 and 55 cm. Accumulation rates decrease down until ca. 0.1 mm yr^{-1} at 25 cm depth. Finally, they increase at their maxima values ranging between 0.6 mm yr^{-1} and >0.8 mm yr^{-1} in the upper 25 cm (Fig. 3), probably mediated by the increasing aquaculture activities (mussel rafts) and the recurrent wood fires (e.g. García-Moreiras et al., 2018).

4.2. MVR-3 grain size, geochemistry, and correlation with the main seismic units

The complete MVR-3 comprised 2.8 m of compacted sediment

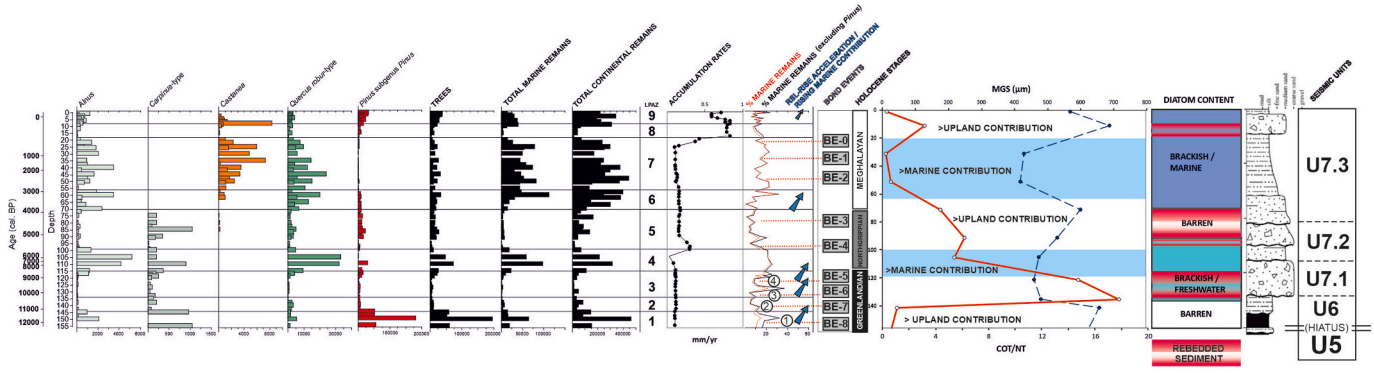

Fig. 5. Changing concentrations of selected tree pollen types, total marine and total continental remains recorded above 155 cm in core MVR-3 sediment, related to accumulation rates, MGS, COT/NT, and diatoms content. Lithology, main Holocene stages and tentative interpretation of seismic units are also shown. Percentages of marine remains and percentages of marine remains excluding *Pinus* are also shown, as compared with stages of increased marine contribution to sediments (eventually related to RSL-rise acceleration at the beginning of the Holocene), and the Bond Events. 1 to 4 represent cold relapses previously described in NW Iberia (Fig. 4; Muñoz Sobrino et al., 2013, 2022; Iriarte-Chiapusso et al., 2016; García-Moreiras et al., 2019a).

(Martínez-Carreño and García Gil, 2017). Its lowest package corresponding to the seismic unit U5 is composed of medium silt and interbedded layers of coarse silt with clear parallel laminations and extends from the base up to 150 cm depth (Fig. 1B). This material includes feldspar, mica, and sub-rounded quartz, but also small gastropods (<1 mm length) and vegetal remains increasing towards its top. Above, between 150 and 137 cm (seismic unit U6), bioclastic remains become rare in the muddy sediment. This abrupt limit has been previously interpreted as a hiatus at ca. 150 cm extending between the Upper Pleistocene and the Early Holocene (Muñoz Sobrino et al., 2018; García-Moreiras et al., 2019a). The combination of the higher resolution (more samples analysed) and the improved chronological model used here suggests that the hiatus may extend more precisely between the Upper Pleistocene (ca. 44 000 cal a BP at >160 cm) and the end of the Younger Dryas (<12 200 cal a BP at 155 cm).

The youngest package (<137 cm, seismic unit U7) is a fining-upward succession consisting of basal bioclastic gravels in a sandy siliciclastic matrix, passing to a mixed bioclastic/siliciclastic sand and sandy mud at the top (Fig. 5). Mean grain size (MGS) notably increases above 140 cm, with maximum medium sizes (>700 µm) between 137 and 100 cm and minimum medium sizes (<20 µm) between 70 and 30 cm and at the top of the sequence. A noticeable increase of MGS (>120 µm) also occurs between 30 and 10 cm (Fig. 5). A TOC/TN ratio lower than 8 usually indicates marine-sourced organic matter and a TOC/TN ratio higher than 12 points to terrestrial source input, whereas a value between 8 and 12 suggests a mixed origin (Goslin et al., 2017; Xia et al., 2022). Measured TOC/TN ratios in MVR-3 persist above 14 in several sections along the sequence but decrease near 12 between 137 and 100 cm and below 11 between 60 and 25 cm (Fig. 5). Thus, these two sections of lower TOC/NT ratios may be related to increases in the proportion of organic matter of marine origin in the sediment, which may be related to increasing marine productivity or lower upland contribution to the sampled fluviomarine sediments.

4.3. MVR-3 pollen, NPP and dinoflagellate cysts analyses (< 155 cm)

Synthetic diagrams are presented in Figs. 4 and 5 that summarise the percentages and concentrations of some selected pollen, dinoflagellate cysts and NPPs types. The sequence can be divided into nine main LPAZ. To avoid further complexity the dinoflagellate cyst dynamics are also described below as following the same pollen zonation. Descriptions refer to total pollen content.

LPAZ-1 (155-143 cm; ca. 12 200 - 11 000 cal a BP) is a wooded phase characterised by very high *Pinus* subgenus *Pinus* percentages (almost 80%) and consistently low evidence (<5%) of other deciduous trees (*Quercus robur*-type, *Alnus*, *Corylus*, *Betula*, *Carpinus*-type), heaths (Ericaceae/*Corema*) and herbs (Poaceae, Amaranthaceae, Asteraceae-Tubuliflorae). Meanwhile, aquatics (mainly *Ranunculus*-type) are scarce, and D/P ratio remains low (<0.2). The dinoflagellate cysts record mainly consists of autotrophic forms (H/A <0.01), with increasing *Spiniferites* spp. (>40%), decreasing *Bitectatodinium tepikiense* (<40%) and relatively low percentages of *Lingulodinium machaerophorum* (20%).

LPAZ-2 (143-136 cm; ca. 11 000–10 500 cal a BP) reveals a noticeable decline in *Pinus* subgenus *Pinus* (<40%) and *Quercus robur*-type increasing (almost 20%). Besides, marsh and coastal vegetation increase (Amaranthaceae, Asteraceae-Tubuliflorae) with Poaceae peaking (almost 30%) and other freshwater-related taxa increasing: *Ranunculus*-type (>20%), *Isoetes*, cf. *Juncus*. The D/P (<0.2) and H/A (<0.07) ratios remain low but *Spiniferites* spp. peaks (>60%) while both *Lingulodinium machaerophorum* (<10%) and *Bitectatodinium tepikiense* (<5%) decline.

LPAZ-3 (136-115 cm; ca. 10 500–8500 cal a BP) indicates the return to a situation like that of the LPAZ-1, with *Pinus* subgenus *Pinus* increasing again (>50%) and *Quercus robur*-type decreasing (<10%), but Poaceae percentages remain usually high (10–30%) and freshwater indicators (*Ranunculus*-type, *Isoetes*, cf. *Juncus*) lightly decaying. Note that this zone includes two peaks (117–120 cm; and 126–132 cm) of *Pinus* subgenus *Pinus,* Ericaceae/*Corema* and Poaceae, respectively dated at ca. 8200 and 9300 cal a BP. Below (ca. 135 cm) another peak of *Pinus* subgenus *Pinus* and Poaceae is older than 10 000 cal a BP. Besides, *Spiniferites* spp. percentages usually retreat, with increasing evidence of both *Lingulodinium machaerophorum* (>30%) and *Bitectatodinium tepikiense* (almost 40%). Nevertheless, D/P (<0.2) and H/A (<0.08) continue stable.

LPAZ-4 (115-99 cm; ca. 8500 - 5800 cal a BP) evidences the retreat of *Pinus* subgenus *Pinus* and the maximum development of *Quercus robur*-type (almost 40%) and other deciduous/riparian trees (*Alnus*, *Corylus*) in the sequence, with Poaceae stabilising around 20% and aquatics (*Ranunculus*-type, *Isoetes*, *Equisetum*) increasing. Foraminiferal linings (>5%) and dinoflagellate cyst abundances quickly increase, the D/P ratio doubles (almost 0.4) and heterotrophic cysts also rise (H/A >0.15). *Lingulodinium machaerophorum* peaks (>70%), *Spiniferites* spp. retreats (<10%) and *Bitectatodinium tepikiense* declines (<5%).

LPAZ-5 (99-70 cm; ca. 5800 - 3800 cal a BP) again indicates conditions as those registered in both LPAZ-1 and LPAZ-3, including new peaks of *Pinus* subgenus *Pinus* (>50%) and the decline of *Quercus robur*-type, *Alnus* and *Corylus* and aquatics, the last except for two peaks of cf. *Juncus*. Besides, this zone includes the last evidence of *Carpinus*-type but also the first discontinuous evidence of *Castanea* pollen registered in the sequence. Dinoflagellate cysts become scarcer, and the D/P ratio returns to low values (0.2), but maxima H/A ratios persist above 0.1. *Lingulodinium machaerophorum* retreats again (<50%), with increasing evidence of *Bitectatodinium tepikiense* (almost 50%) and *Spiniferites* spp.

(with a peak of >40%).

LPAZ-6 (70-56 cm; ca. 3800 - 3000 cal a BP) reveals the total tree pollen retreating (<40%), basically due to the *Pinus* subgenus *Pinus* decline (<20%), because other trees as *Quercus robur*-type (>20%) and *Alnus* increase, and the continuous *Castanea* pollen curve starts at 65 cm, dated at ca. 3400 cal a BP. Besides, the first evidence of Cerealia-type appears simultaneously, and some herbs (Poaceae >30%; Asteraceae-Tubuliforae >5%) and aquatics (*Ranunculus*-type) increase. The D/P ratio quickly rises (0.5) at the same level (65 cm) when the highest H/A values (>0.3) of the sequence are registered. *Lingulodinium macherophorum* predominates with values oscillating between 30 and 80% (and clearly increasing at 65 cm depth), and *Bitectatodinium machaerophorum* (<10%) and *Spiniferites* spp. (<5%) retreating.

LPAZ-7 (56-18 cm; ca. 3000 - 200 cal a BP) corresponds to a period of almost three millennia characterised by the lowest tree pollen percentages, with *Quercus robur*-type oscillating (10–30%) but *Pinus* subgenus *Pinus* remaining below 5%. Parallel, a continuous *Castanea* pollen curve is recorded that rises above 10% before 1000 cal yr BP, with maximum percentages of Ericaceae/*Corema* (>10%), Poaceae (>40%) and *Pteridium* (>10%), and the development of the Cerealia-type pollen curve. Besides, *Zea mays* was introduced at the top of this zone. Several peaks (>20%) of aquatics (mainly cf. *Juncus*) appear during the first half of this zone. *Lingulodinium machaerophorum* (>70%) dominates the dinoflagellate cyst record, while the D/P ratio oscillates but remains consistently high (0.3–0.5). Two H/A relative maxima (>0.16 and > 0.1 at 44 and 24 cm, respectively) are recorded that correspond to the two relative D/P minima found.

LPAZ-8 (18-10 cm; ca. 200 - 90 cal a BP) indicates modern afforestation with pines (>50%) and *Eucalyptus*, and a reduction of Ericaceae/*Corema* (10%) and Poaceae (10%). Besides, cf. *Juncus* increases but the total aquatics retreat. The D/P and H/A ratios decrease to almost 0.1 and 0.05 respectively, and *Bitectatodinium tepikiense* peaks (>30%) while *Lingulodinium machaerophorum* retreats (30%).

LPAZ-9 (10-0 cm; ca. 90 to −50 cal a BP). Afforestation with pines and *Eucalyptus* continues, with *Castanea* pollen peaking (>20%). *Quercus robur*-type reaches its minimum values recorded since the Early Holocene, with increases in heaths (Ericaceae/*Corema, Calluna*), herbs (Poaceae) and aquatics (*Ranunculus*-type). The D/P ratio increases again (almost 0.3), with an H/A peak (>0.01) at the base of this zone and, subsequently, *Lingulodinium machaerophorum* rising again up to 75%.

4.4. MVR-3 diatom evidence

Five of the seventeen samples studied lack appreciable diatom content (Table 3; Plate 1; Fig. 6). Those barren samples correspond to two different sections of sediment, the deepest levels (144–155 cm) and an intermediate 70–90 cm section. The sediment between both barren sections (100–135 cm) is characterized by the common occurrence of species with brackish and freshwater ecologies, with some samples (e.g. 110–111 cm and 114–115 cm, Table 3) clearly including benthic freshwater species (*Nitzschia* aff. *inconspicua*, *Cocconeis* aff. *euglypta, Reimeria sinuata* and *Gomphonema* sp.) mixed with other cosmopolitan, markedly euryhaline species (*Cocconeis* sp. and *Nitszchia* aff. *frustulum*). Diatoms composition notably changes in the upper part of the sediment core (<61 cm), with most of the samples including brackish or fully marine species such as: *Actinocyclus* sp., *Actinoptychus senarius, Biddulphia antediluviana, Cyclostephanos* sp. and *Grammatophora* sp. (Table 3; Plate 1; Fig. 6), some of them widespread in marine littoral and coastal areas (Round et al., 1990; Witkowski et al., 2000).

4.5. Reworked pollen estimated per LPAZ

Analyses performed (Table S2) suggest that percentages of rebedded pollen (mainly *Pinus* subgenus *Pinus* and *Erica*) vary between ca. 16% in the LPAZ-2 and ca. 30–38% in the LPAZ-3 to LPAZ-8 (Fig. 4). Radiocarbon dates obtained from pollen residues are only clearly anomalous in those levels with unexpected pine pollen peaks (LPAZ-2, LPAZ-3, LPAZ-5) in which the contribution of recycled material (see average % of *Pinus* pollen per LPAZ in Table S2) has been estimated to be the highest (Fig. 3).

Table 3
Diatoms content of core MVR-3, showing the main species at the different depths analysed and their preferred environments.

Depth (cm) MRV-3	Diatom species	Ecology of diatom species
0–1	*Cocconeis* sp., *Diploneis* sp. and *Melosira* sp.	Brackish/Marine
10–11	*Cyclotella meneghiniana* and *Staurosirella pinnata*	Brackish/Marine
20–21	*Actinocyclus* sp., *Actinoptychus senarius, Biddulphia antediluviana, Cocconeis* sp., *Cyclostephanos* sp., *Diploneis* aff. *stroemii, Ehrenbergia* sp., *Grammatophora* sp., *Planothidium frequentissimum* and *Rhoicosphenia* sp.	Brackish/Marine
29–30	*Cocconeis scutellum* and *Ehrenbergia* sp.	Brackish/Marine
40–41	*Actinoptychus senarius, Aulacoseira* sp., *Cocconeis* sp., *Ehrenbergia* sp., *Fragilaria* sp. and *Nitzschia* sp.	Brackish/Marine
50–51	*Actinoptychus senarius*	Brackish/Marine
60–61	*Actinoptychus senarius* and *Diploneis* sp.	Brackish/Marine
70–71	ø	ø
80–81	ø	ø
89–90	ø	ø
100–101	*Amphora* aff. *pediculus, Gomphonema* sp. and *Reimeria uniseriata*	Brackish/ Freshwater
110–111	*Cocconeis* aff. *euglypta, Cyclotella* sp., *Gomphonema* sp. and *Reimeria sinuata.*	Brackish/ Freshwater
114–115	*Diploneis* sp., *Gomphonema* sp., *Nitzchia* aff. *frustulum* and *Rhoicosphenia* sp.	Brackish/ Freshwater
125–126	*Cyclotella meneghiniana* and *Nitzchia* aff. *inconspicua*	Brackish/ Freshwater
134–135	*Amphora* aff. *pediculus, Caloneis* sp., Cocconeis sp., *Fragilaria fascitulata* and *Nitzschia* sp.	Brackish/ Freshwater
144–145	ø	ø
155–156	ø	ø

4.6. Analyses of differences between pine pollen total grain sizes

The total *Pinus* pollen grain concentrations (Fig. 6) and average sizes notably oscillate across the record (Fig. 7; Table S3), with the lowest means (<62 μm) found in LPAZ 1 and LPAZ-8; the highest (>68.5 μm) in LPAZ-9, LPAZ-7, and LPAZ-4, and intermediate values in the rest (Fig. 7). Descriptive statistics (Table S4) and normality tests performed (Table S5) after discarding statistically significant outliers (Grubbs test) indicate the total grain sizes of pine pollen differ from normal distribution in LPAZ-1, LPAZ-2, LPAZ-5, LPAZ-7, and LPAZ-8. Besides, the hierarchical cluster analysis (Fig. 7B) agrees in differentiating pollen zones LPAZ-9, LPAZ-7, and LPAZ-4 from the others, dividing the last into two clades: LPAZ-1, LPAZ-3, LPAZ-6, and LPAZ-8 in the first cluster; and LPAZ-2 and LPAZ-5 in the second (Fig. 7B). All the non-parametric pairwise tests (Table S6) reveal significant differences between: LPAZ-1 and LPAZ-9, LPAZ-7, and LPAZ-4; but also, between LPAZ-4 and LPAZ-8; between LPAZ-7 and LPAZ-8; and between LPAZ-8 and LPAZ-9. Mann–Whitney and Dunn's post hoc tests also agree, pointing to LPAZ-9 as being significantly different from LPAZ-8, LPAZ-6, LPAZ-5, LPAZ-3, LPAZ-2, and LPAZ-1; and LPAZ-8 from LPAZ-3, LPAZ-4, LPAZ-5, LPAZ-6, and LPAZ-7 (Fig. 7; Table S6).

5. Discussion

5.1. Postglacial climate, RSL and hydrological changes

The climatic pattern over the North Atlantic dramatically changed in the transition from the Last Glacial Maximum (LGM) to the postglacial period (e.g. Justino and Peltier, 2005; Heiri et al., 2014; Matero et al.,

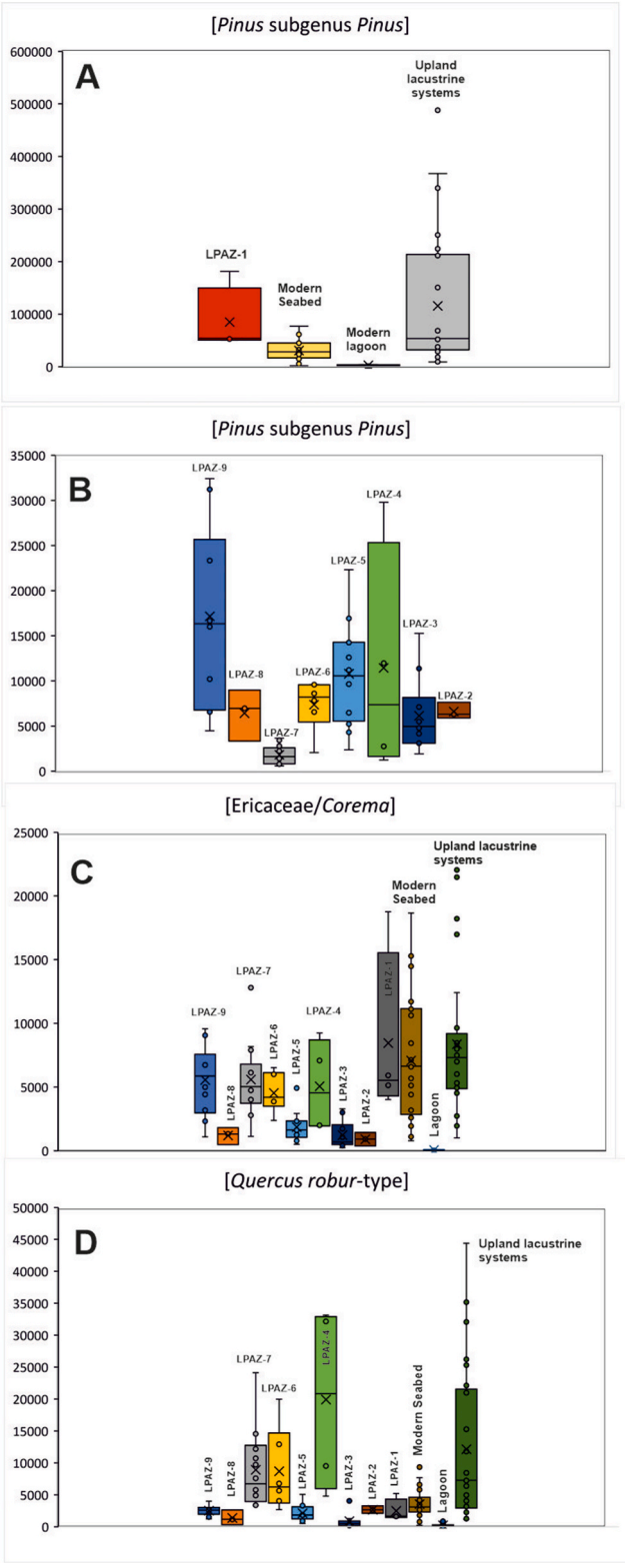

Fig. 6. Boxplots representation of A) *Pinus* subgenus *Pinus* concentrations (grains/cm^3) in LPAZ-1 (MVR-3) in relation to *Pinus* pollen concentrations recorded in different modern sediment samples (see Fig. 2BC); B) *Pinus* subgenus *Pinus* concentrations (grains/cm^3) changing in the different LPAZ identified in core MVR-3; C) Ericaceae/*Corema* concentrations (grains/cm^3) changing in the different LPAZ identified in core MVR-3, and compared with *Erica* pollen concentration in modern sediment samples (see Fig. 2BC). D) *Quercus robur*-type concentrations (grains/cm^3) changing in the different LPAZ identified in core MVR-3.

2017; Rea et al., 2020; Max et al., 2022) and, particularly, the rapid climatic variation of the Lateglacial/Holocene transition in NW Iberia (e.g. Muñoz Sobrino et al., 2013; Iriarte-Chiapusso et al., 2016) also affected the temperate eastern Atlantic coastal upwelling systems (e.g. Abrantes, 1991; García-Moreiras et al., 2019a, 2019b; Muñoz Sobrino et al., 2022). Evidence of high-frequency climate variability over the North Atlantic extends throughout the Holocene in the North Atlantic and European regions (Bond et al., 1997; Wanner et al., 2015), presumably connected to the advection of southward and eastward drifting surface water from the Nordic and Labrador Seas, which gave rise to century-scale cold relapses (Bond Events, BE). The postglacial climate oscillations impacted the volume of continental ice and changed the sea level.

Available data from NW Iberia (e.g. Dias et al., 2000; Leorri et al., 2013; Martínez-Carreño and García-Gil, 2017) point to a phase of rapid sea-level increase, from −130 m (relative to present sea level) at the Last Glacial Maximum (GS-2, Björk et al., 1998) to about −26 m at the beginning of the Holocene (11.2–9.4 cal ka BP). High-quality relative sea-level data (including standardised vertical uncertainties) available for the Atlantic coast of SW Europe indicate that RSL remained below present during the Holocene, with a rapid rise (rates of RSL change around 6.3 mm yr^{-1}) from 10 to 7 ka, with the Mid-to late-Holocene rates decreasing down to 0.9–0.1 mm yr^{-1}, depending on the latitude, with also a number of limiting dating available for the Galician coast (García-Artola et al., 2018, Fig. 8). The regional RSL and rates of change reconstructed for the Holocene may also be related to the modifications affecting different marine/terrestrial transition ecosystems. Changes affecting these ecotones have been largely described in several locations of the Galician Atlantic coast as mediated by a combination of climatic and anthropogenic factors (e.g. Costas et al., 2009; Leorri et al., 2013; Muñoz Sobrino et al., 2014; 2016, 2022; González-Villanueva et al., 2015; Sáez et al., 2018; Cajade-Pascual et al., 2023; Gardoki et al., 2023).

Muñoz Sobrino et al. (2022) precise several stages of in situ development of salt marsh and freshwater/brackish pond vegetation in Ría de Ferrol (Fig. 1A), which provide additional insight into the sea-level changes in the Galician rias (Fig. 8). In detail, it places the sea level during the Younger Dryas largely below −21.4 ± 0.7 m (after adding an error range for sampling uncertainty, core shortening and water depth uncertainty following García-Artola et al., 2018). Deposits from freshwater/brackish ponds during the early Holocene that can be attributed to the 11.4, 10.5, 9.3 cal ka BP episodes correspond to terrestrial limiting indicators pointing to a sea level below −21.4 ± 0.7 m, −21.1 ± 0.7 m and −13.2 ± 0.7 m, respectively (Fig. 8). Saltmarsh vegetation developed at 8.5–8.9 cal ka BP and 7.8–8.1 cal ka BP indicates a sea-level position of −21.21 ± 1.8 m and −13.9 ± 1.8 m, respectively (Fig. 8, converted to sea-level index points using the indicative meaning ranges from García-Artola et al., 2018). Thus, all of them may be linked to successive Bond events, i.e., the BE-8, BE-7, BE-6, and BE-5, respectively (e.g. Bernal-Wormull et al., 2023). Furthermore, previous reconstructions obtained in nearby coastal areas (Pena et al., 2010) but also in RdV (Muñoz Sobrino et al., 2007, 2012, 2014, 2016; García--Moreiras et al., 2018) described some short relapses (Figs. 4 and 5) that may be coupled to the more recent Bond events, namely the BE-0 (Little Ice Age, ca. 0.5 ka BP), the BE-1 (Late Antique Little Ice Age, 1.4 ka BP), the BE-2 (the Iron Age Cold Period, ca 2.8 ka BP) and the BE-3 (ca, 4.2 ka BP). The new data discussed here (Figs. 4 and 5) documents for the first time the complete postglacial record in fluviomarine sediments from NW Iberia and includes conclusive evidence of the BE-4 (ca. 5.9 ka BP) in RdV that enables to discuss its environmental implications.

Climate and sea level rise also determine mayor hydrological changes that are recognisable in core MVR-3. Between 100 and 135 cm diatoms identified are mainly benthic brackish and freshwater species (Fig. 6), which indicates upland contribution from rivers and sea-shore transition ecosystems, most probably developed in ancient lowlands that stayed emerged when the relative sea level was low (Fig. 8). Diatoms are

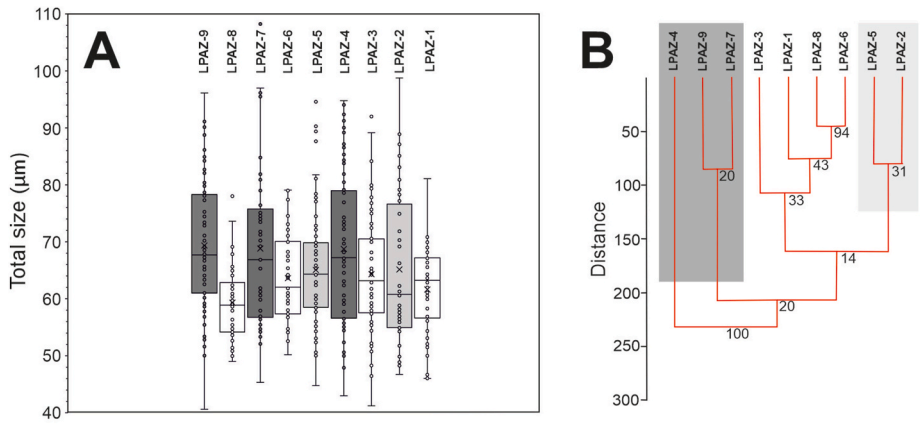

Fig. 7. A) Boxplot representing *Pinus* subgenus *Pinus* sizes in registered during the last 12 000 years in the different LPAZs of the core MVR-3. Tables in S3, S4 show the results of the significant differences analyses performed. B) Results of the cluster analysis performed, using Ward's algorithm, the Euclidean similarity index and 9999 boots.

almost absent in the sediment during the periods ca. 10 000–11 000 cal BP and ca. 4000–6000 cal BP, coinciding with anomalous peaks of *Pinus*. These correspond to drier phases (i.e., lower contribution of brackish and freshwater diatoms), with lower accumulation of diatoms and dinoflagellate cysts, which are poorly preserved in the sediment. This last may be explained by a combination of factors, namely mixed waters, with the seabed being more oxygenated and diatoms being predated by more abundant heterotrophic cysts (Fig. 4B). Heterotrophic dinoflagellates have lower cyst production capabilities compared to those of *Lingulodinium polyedrum* (Figueroa and Bravo, 2005), which also contributes to the decreasing accumulation of total dinoflagellate cysts (Fig. 4).

The H/A ratio largely remains below 0.12 in most of the MVR-3 samples analysed except for four stages (1–4 in Fig. 4B) respectively dated at ca. 7700 cal a BP (>0.15), ca. 3500 cal a BP (0.34), ca. 2000 cal a BP (0.16), and the early 20th century (0.14). All of them correspond to transition phases from stratified to prevailing mixed marine waters when the continental contribution (aquatics) to the sediment notably peaks. The highest H/A ratio at ca. 3.5 ka BP matches with the moment when the hydrological conditions of the middle part of the ria definitively adopted its modern configuration and behaves like a weakly stratified semi-enclosed bay (Barton et al., 2015), with increasing evidence of brackish/marine diatoms in the sediment (Fig. 5). But also matches with the phase of strongest deforestation of the basin during the Holocene, which may be related to the regional development of agriculture (Figs. 4 and 5). In the Atlantic Galician rias, these conditions can be linked to increased eutrophication and primary production (Rego, 2022; Ospina-Alvarez et al., 2014).

5.2. Multiproxy evidence of postglacial environmental changes

Major environmental changes that occurred in RdV throughout the postglacial period, as deduced from the high-resolution multiproxy evidence available (Figs. 4–9), are synthesised below following the formal Holocene subdivision and discussed in relation to other regional evidence available.

5.2.1. Greenlandian Stage (11.7–8.3 ka)

The combination of higher-resolution pollen data and the improved chronological model indicate that the section of MVR-3 between 155 and 115 cm corresponds to the Greenlandian Stage (LPAZ-1 to LPAZ-3; Figs. 4, 5, 8 and 9), i.e., the Early Holocene extending from <11.7 to 8.2 ka (Fletcher et al., 2024). A hiatus may be established at ca. 155–160 cm corresponding to the boundary between seismic units U5 and U6. Therefore, the Greenlandian stage is included in seismic units U6 and U7.1 of RdV (Fig. 5). Nevertheless, the boundaries of U7 seismic subunits may be considered probable but tentative, because the seismic evidence in the shallow margins of the basin is on the limits of the resolution. Thus, further high-resolution studies will be needed (in other parts of the basin where those seismic subunits are thicker) to refine them.

Accordingly, the studied MVR-3 sequence (0–155 cm) starts in the transition between the Younger Dryas and the 11.4 ka cold event (BE-8) when the RSL was below −20 m (García-Artola et al., 2018; Muñoz Sobrino et al., 2022, Fig. 8C). Consistently, LPAZ-1 is characterised by the notable abundance of dinoflagellate cysts but, particularly, by high accumulation rates of microremains of continental origin (Fig. 9B), including pollen (mainly *Pinus* subgenus *Pinus* and Ericaceae/*Corema*) and animal, algal and fungal remains (Fig. 6). This evidence is coherent with the occurrence of pinewoods and heath developing on the coastal lowlands of Ría de Arousa (Fig. 1A) during the Lateglacial Interstadial/Early Holocene transition (García-Moreiras et al., 2019b).

The regional summer mean temperature rose about 2 °C in NW Iberia between 12 500 to 10 500 cal a BP, with the estimated July air temperature in the coastal areas reaching 21.5 °C (Heiri et al., 2014; Muñoz Sobrino et al., 2022). Thus, the rising evidence of deciduous oaks and aquatics in LPAZ-2 reveals an increase in regional temperature and precipitation (Fig. 4), with the associated increases in Amaranthaceae, Poaceae, cf. *Juncus* and Asteraceae, indicating a higher representation of coastal wetlands and dunes as the sea level rapidly rose (Fig. 9C), with more than 10 m of rise estimated in two millennia (García-Artola et al., 2018; Muñoz Sobrino et al., 2022).

LPAZ-3 (ca 10 500–8500 cal a BP) is a relatively colder phase, with RSL remaining below −12 m (Fig. 8C; García-Artola et al., 2018; Muñoz Sobrino et al., 2022) and characterised by low accumulation rates of both marine and continental remains (Figs. 4 and 5). This unstable period (Fig. 9D) may be understood as the succession of three brief episodes of cooling that interrupted the regional expansion of deciduous *Quercus* during the Early Holocene (Fig. 4). They have been dated at ca. 10.5, 9.3 and 8.2 ka and therefore are probably connected to BE-7, BE-6, and BE-5, respectively. This evidence is consistent with previous reconstructions performed for this period in other fluviomarine and continental sedimentary systems in NW Iberia (Pena et al., 2010; Iriarte-Chiapusso et al., 2016; García-Moreiras et al., 2019a; Muñoz Sobrino et al., 2022).

5.2.2. Northgrippian stage (8.3–4.3 ka)

Mid-Holocene sediments in the shallower margins of RdV are probably packaged in seismics subunits U7.1 to U7.2, but the boundary between both subunits in the site where MVR-3 was collected is only tentative because of the low thickness of the sediments at this point (Fig. 5). This stage includes the LPAZ-4 and the LPAZ-5 (Fig. 5). LPAZ-4

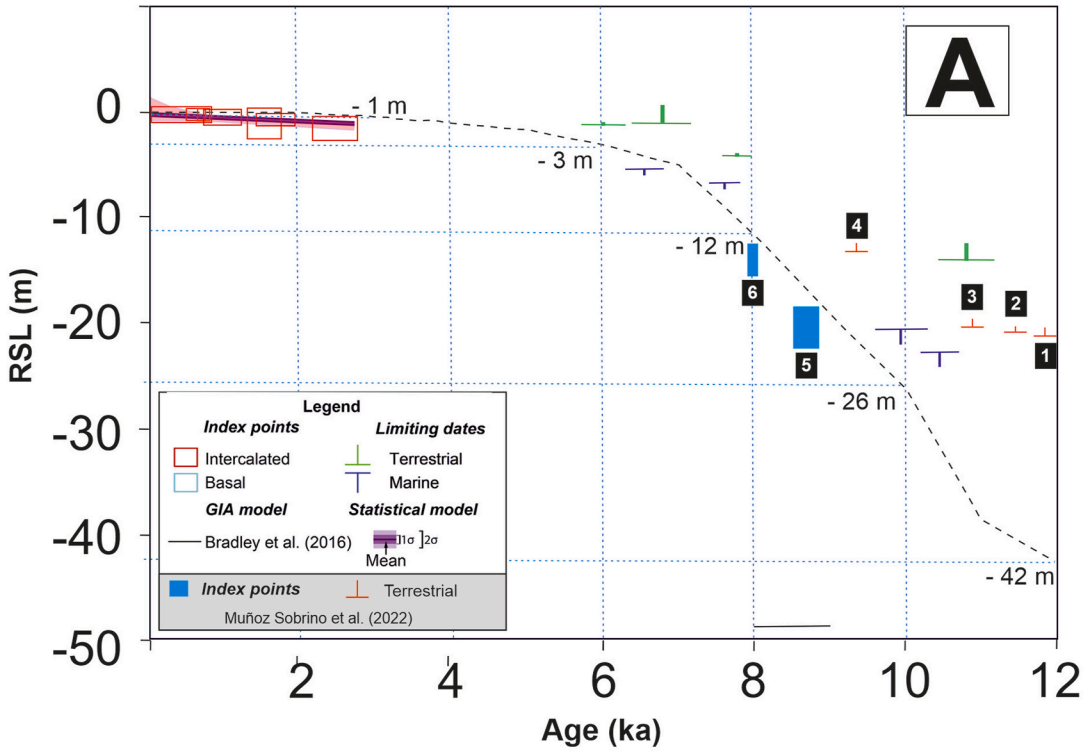

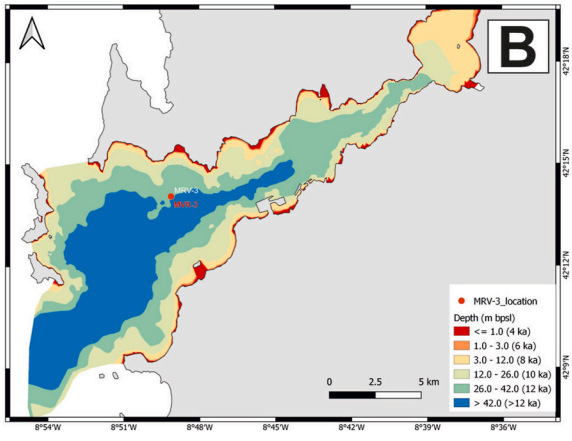

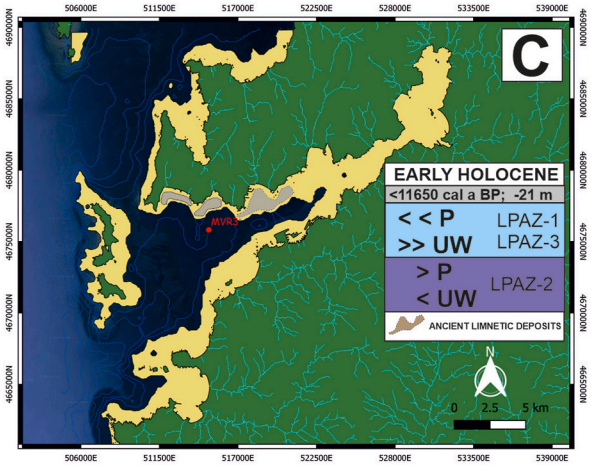

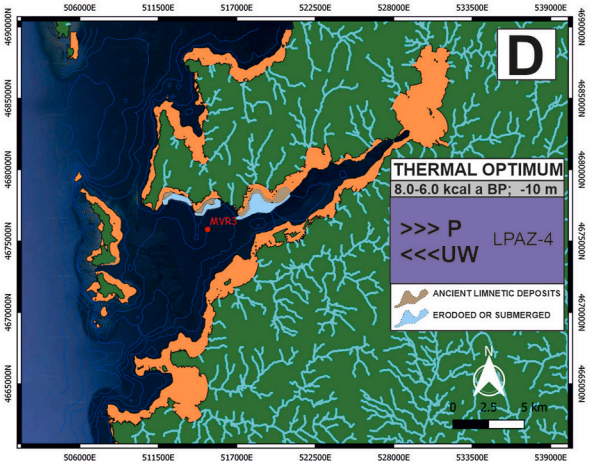

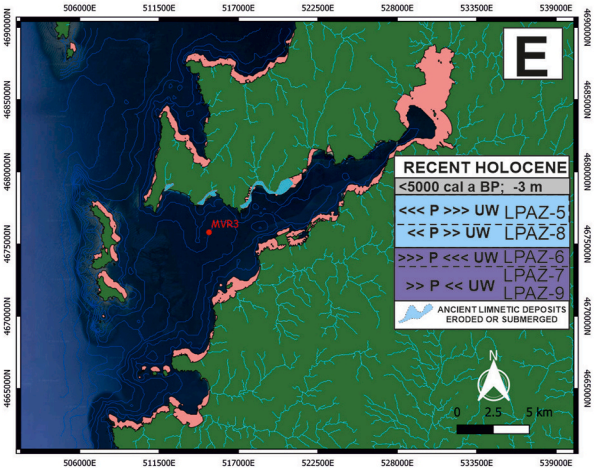

(caption on next page)

Fig. 8. (A) RSL curve of Bradley et al. (2016) with evidence discussed in García-Artola et al. (2018), and new index points and terrestrial limited dates incorporated from Muñoz Sobrino et al. (2022). In the Galician Atlantic coast, nine limiting dates (eight marine, one freshwater) constrain RSL to above −38.2 m at ~10.9 ka and −36.2 m at ~10.6 ka. Later, RSL rose from −21.7 ± 2.3 m at 9.6 ka, to −9.5 ± 2.1 m at ~8.4 ka and reached −4.1 m at ~7 ka (i.e., a rate of 4.7 ± 0.8 mm yr^{-1}). Subsequently, marine and terrestrial limiting dates constrain RSL to below −0.7 ± 1.8 m at ~5 ka, to above −3.2 ± 1.8 m at 4.4 ka and −1.9 m at 3.1 ka. More recently, RSL rose from −1.8 ± 21 m at ~2 ka to −0.2 ± 2.1 m at ~0.9 ka, i.e. a rate of 0.6 ± 0.7 mm yr^{-1} during the last two millennia (García-Artola et al., 2018). 1 to 4 are four limiting terrestrial dates that respectively corresponds to the YD, and the 11.4, 10.5, 9.3 cal ka BP episodes. The index points 5 and 6 respectively represent saltmarsh vegetation developed at 8.5–8.9 cal ka BP and 7.8–8.1 cal ka BP; (B) Marine transgression in Ría de Vigo according to the age-depth model proposed in García-Artola et al. (2018), and the seismic data and marine levels discussed in Martínez-Carreño and García-Gil (2017). Reconstruction of Ría de Vigo during (C) the Early Holocene with the palaeocoast at −21 m; (D) the Thermal Optimum with the palaeocoast at −10 m, and (E) the recent Holocene with palaeocoast al −3 m. To produce figures C, D and E the modern isobaths were used, but also according to the evidence (showed in A), described in García-Artola et al. (2018), Muñoz Sobrino et al. (2022), and Martínez-Carreño et al. (2017). P: precipitation; UW: upwelling.

indicates the maximum development of deciduous forests (*Quercus robur*-type, *Alnus*, *Corylus*), and has been dated between ca. 8000-6000 cal a BP (Figs. 4, 5 and 8D and 9E). This phase also coincides with the Holocene Climatic Optimum (Thermal Maximum) described in northern Iberia (e.g. Muñoz Sobrino et al., 2005; Bernal-Wormull et al., 2023) and agrees with the reconstructions of vegetation dynamics available both in the coastal uplands (e.g. Gomez-Orellana et al., 1998; 2021) and the oceanic mountains from NW Iberia (e.g. Muñoz Sobrino et al., 1997, 2001; Iriarte-Chiapusso et al., 2016). Besides, the noticeable increase in D/P (Fig. 4) also supports the increase in marine influence. Another relevant characteristic of this zone is the higher accumulation rates, which may be primarily related to the warmer and wetter conditions. The increasing evidence of *Lingulodinium machaerophorum* indicates the weakening of the upwelling (Prego et al., 2024) and thus low oxygenation of the seabed. Thus, the better preservation of remains in the sediment may also help explain the accumulation rates and D/P ratio increase (Fig. 4).

LPAZ-5, dated between ca. 6000-4000 cal a BP, is characterised by increases in *Pinus* subgenus *Pinus,* low contribution of aquatics, a noticeable retreat in *Lingulodinium machaerophorum* and lower accumulation rates (Figs. 4, 5 and 8D and 9F). These data reveal a period of scarcer precipitations and intensified water mixing in RdV, a picture that fits into the general context described in North Iberia. In hyperoceanic ombrotrophic bogs of the Cantabrian coastal mountains, Muñoz Sobrino et al. (2005) described a period (ca. 6.0–4.0 ka BP) of more variable but generally lower temperatures, while in the western Pyrenees, Bernal-Wormull et al. (2023) found a cold dry period dated between 6.0 and 2.5 ka BP. Besides, in many small lakes and peat bogs in the NW Iberia mountains and the Duero depression, erosion increases and even sedimentation is eventually interrupted between 6.0 and 4.0 ka BP (Muñoz Sobrino et al., 1997, 2001, 2004;Ramil Rego et al., 1998; Morales-Molino et al., 2013; Iriarte-Chiapusso et al., 2016; van der Horst et al., 2024), while Benito et al. (2023) describes that during the Mid-Holocene the Duero basin lacks flooding evidence. Parallel, Jiménez-Moreno et al. (2023) identified a rapid cooling (~1.5 °C) in southern Iberia that extended between ca. 7.2 and ca. 3.0 cal ka BP. Vegetation changes with increasing of *Betula* and heathlands also occurred during this period in the oceanic mountain areas of NW Iberia, which has been usually attributed to a combination of climate and human activity (e.g. Muñoz Sobrino et al., 1997, 2005). Accordingly, this Mid-Holocene episode might be a cooler and drier stage that probably affected most of the Iberian Peninsula.

5.2.3. *Meghalayan stage (<4.3 ka)*

The boundary between seismic subunits U7.2 and U7.3 at ca. 80 cm depth is evident in core MVR-3 and is marked by an erosive surface delimiting the change in sedimentary facies from bioclastic sand/gravel to muddy sand (Fig. 1). The increase in accommodation space due to the rise of sea level and/or changes in the hydrodynamic conditions allowed the preservation of a more continuous sedimentary record of subunit U7.3. This limit can be correlated to the modern phase with the greatest contribution of material of marine to the sediment (Fig. 5).

The interval 4000-3000 cal a BP in RdV (LPAZ-6) evidences the transition from stratified to mixed waters, which constitutes the most significant change recorded in the hydrological conditions in RdV during the Holocene (Figs. 4, 5 and 8E and 9G). Meanwhile, *Pinus* subgenus *Pinus* declines, with increasing evidence of heath and herbs (Poaceae, Asteraceae Tubuliflorae), and the first signals of early cultivations (Cerealia-type, *Castanea*) related to the beginning of the anthropogenic deforestation of the basin. This tendency accentuated in the following LPAZ-7, dated ca. 3000- 200 cal yr BP (Figs. 4, 5 and 8E and 9H).

Glacial refugia for *Castanea* may persist in the Eurosiberian coasts of NW Iberia (Fernández-López et al., 2021; Gómez-Orellana et al., 2021) but since the last millennium BC the trend of *Castanea* is mainly attributable to cultivation and arboriculture, probably also promoted by cabotage maritime commercial relationships (Krebs et al., 2022). The earliest pollen evidence of Cerealia-type and *Castanea* has been dated in the innermost part of RdV between 3500 and 3000 cal a BP (Muñoz Sobrino et al., 2012). Later, they consistently developed during the first millennia (Muñoz Sobrino et al., 2014; López-Merino et al., 2023) and finally experienced a noticeable increase across the ria after ca. 1500 cal a BP (Muñoz Sobrino et al., 2014; 2016; López Merino et al., 2023). The same trend, including the maximum regional development of *Castanea* dated between ca. 1200-600 cal yr BP, i.e. the Mediaeval Climate Anomaly (Muñoz Sobrino et al., 2014), can also be identified in the independently dated new MVR-3 record (Figs. 4 and 5).

On the other hand, during the last 3000 years, *Lingulodonium machaerophorum* dominated the dinoflagellate cysts record, and accumulation rates in the sediment persist high, except for a short phase (LPAZ-8; Figs. 4, 5 and 9I), which may be related to the regional evidence of the Little Ice Age (Muñoz Sobrino et al., 2014; 2016; García--Moreiras et al., 2018). The noticeable changes observed in relative abundances and accumulation rates of aquatics, and particularly of cf. *Juncus* (Fig. 4), are consistent with increasing precipitation, river inputs and runoff during those wet stormy periods when *Lingulodinium machaerophorum* and total dinoflagellate cysts accumulation rates increase (Fig. 4). Finally, modern afforestation of the basin occurred in several steps during the last 200 years (LPAZ, 8 and LPAZ-9; Figs. 4, 5 and 9IJ).

5.2.4. *Evidence for reworked pollen*

Major landscape transformations onshore RdV (cultivations, deforestation of the basin, heath expansion, repopulations with *Pinus* and *Eucalyptus*, *Castanea* dynamics) may be successfully identified upon pollen data obtained in the core MVR-3, and their chronologies are also consistent with the historical data and other evidence described in coastal NW Iberia (e.g. Desprat et al., 2003; Muñoz Sobrino et al., 2012, 2014,2016; García-Moreiras et al., 2018; Gómez-Orellana et al., 2021; López Merino et al., 2023). Using pollen evidence, it is also possible to identify certain cold (YD/11.4, 10.5, 9.4, 8.2) and warm (Climatic Optimum, Mediaeval Climate Anomaly) periods previously described in this region (Moreno et al., 2014; Heiri et al., 2014; Iriarte-Chiapusso et al., 2016; Muñoz Sobrino et al., 2014; 2016, 2022). Nevertheless, several anomalous pollen successions exist during the Holocene that were not identified in the area before (e.g. Gomez-Orellana et al., 1998; Kaal et al., 2011; Muñoz Sobrino et al., 2012; García-Moreiras et al., 2019a), with *Pinus* repeatedly peaking when *Lingulodinium* declines.

Differential dating reveals that those periods with anomalous pollen

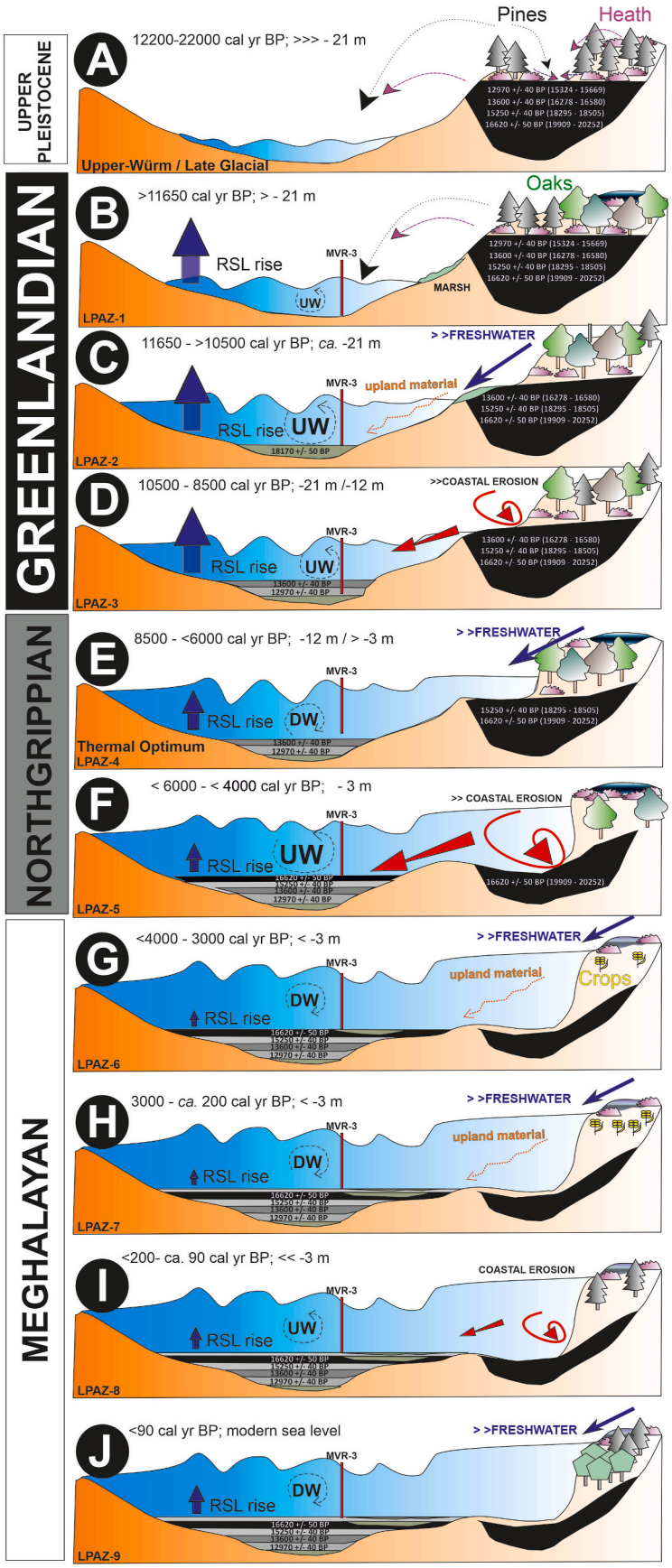

Fig. 9. Conceptual model explaining in ten phases (from A: Upper Würm/Lateglacial transition to J: last century) the major sea-level changes (see Fig. 8), environmental oscillations, and chronological anomalies detected in core MVR-3, Ría de Vigo, NW Iberia (see the text). UW: upwelling intensification; DW: Downwelling prevailing. The size of the symbols refers to the intensity of the process.

successions show conspicuously aged pollen chronologies, which according to the event stratigraphy of Björk et al. (1998), corresponds to several cold stages (Fig. 3) dated between the Greenland Interstadial 2 (GI-2: >21,8 cal ka BP) and the Greenland Interstadial 1e (GI-1e: <14.7 cal ka BP). Besides, these dated levels are apparently inverted (Fig. 3).

These facies may constitute evidence of redeposition of ancient upland sediments, formed above the palaeo-coastline at different intervals comprised between the end of the LGM and the early stages of the Lateglacial (Figs. 8 and 9). Therefore, most of the pollen evidence recorded in these facies (mainly *Pinus* subgenus *Pinus*) was reworked and resedimented in an orderly manner during the periods with the highest rate of the RSL (García-Artola et al., 2018), i.e., at the start of the early Holocene (12.0–8.0 cal ka BP; Fig. 8), but also in the interval between ~6.0 and ~4.0 cal ka BP (Figs. 5 and 8). The weather conditions interpreted for this last stage may be only sporadically stormy (i.e., it was a dry and relatively cold period, with moderate contribution of materials of terrestrial origin towards the saltmarshes and other coastal ecosystems associated with them), but simultaneously it was also a period characterised by enhanced upwelling and prevailing stratified waters (i.e., with low contribution of *Lingulodinium machaerophorum*). Thus, the input of contemporary materials of marine origin was also limited (Fig. 6) due to the lower dinoflagellate cyst production and worse preservation (more oxygenation of the bottom). Therefore, there is a delay in the pollen evidence between the two main phases of high marine influence at ca. 11.0–8.2 cal ka BP and 4.0-3.0 ka BP (Fig. 5) and the two subsequent warm stages: the Climatic Optimum (8.0–6.0 cal ka BP) and the 2.5–0.5 cal ka BP interval, respectively.

The *Pinus* subgenus *Pinus* and Ericaceae/*Corema* pollen concentrations found in LPAZ-1 are much higher than equivalent pollen concentrations recorded in 10 samples of sediment from a modern lagoon in the Cíes Islands (Figs. 2 and 6; Muñoz Sobrino et al., 2016; Castro-Parada et al., 2023) and those of 26 modern seabed sediment samples recorded across RdV (Fig. 2 and 6; Castro-Parada et al., 2023). Nevertheless, they fit in the range of concentrations found in 20 modern samples of sediment taken in nearby upland lacustrine systems (Figs. 2 and 6; Castro-Parada and Muñoz Sobrino, 2022), which suggest that pinewoods and heath formed part of upland ecosystems developing around RdV at the beginning of the Holocene, as it happened in other coastal areas from NW Iberia (García-Moreiras et al., 2019a; Cartelle et al., 2022; Muñoz Sobrino et al., 2022). Concentrations of *Pinus* subgenus *Pinus* notably decline in the pollen zones above, and only in the LPAZ-9 (modern repopulations) and the LPAZ-4 (Thermal Optimum) there is an increase up to values that are comparable to those in modern seabed sediment (Fig. 6). Particularly, *Pinus* pollen concentrations steadily decrease from LPAZ-5 to LPAZ-7, where concentrations of pine pollen are minimal (Fig. 6) but still higher than those of *Quercus robur*-type, which instead increases from LPAZ-5 to LPAZ-7. These trends strongly suggest that most of the *Pinus* subgenus *Pinus* pollen evidence from LPAZ-3 and LPAZ-5 has been reworked and resedimented in the seabed during the Holocene marine transgression.

The change in colour intensity and pollen oxidation in sediments depends on the increasing maturity of the samples (Yule et al., 1998; Traverse, 2008) and on the processes of transport and sedimentation involved (Moore et al., 1991). Most of the redeposited microfossils are dark in colour due to physicochemical changes and can differ in preservation, the gymnosperm pollen being the best preserved (e.g. Kvavadze, 1996). Nonetheless, the colour and preservation status probably underestimate the rebedded pollen in our postglacial fluviomarine sedimentary systems, in view that most of the pollen resedimented is highly resistant bisaccated pollen that was originally deposited, only a few thousand years before, in nearby coastal wetlands. In climates with noticeable rainfall fluctuations, the abundance of fungal hyphae (interpreted as washed plant litter) has been used as an index of the rebedded pollen redeposition (Cushing, 1964; López-Merino et al., 2016). Nevertheless, the anomalous *Pinus* peaks in MVR-3 are inversely proportional to the enhanced runoff (aquatics) and seem to be independent of the abundance of fungal remains. (Figs. 4 and 10A).

Comparative size analyses (Fig. 7; Table S6) of the *Pinus* subgenus *Pinus* pollen found in the different pollen zones reveal that the total grain sizes in LPAZ-1 to LPAZ-3 are significantly different (smaller) than those corresponding to the modern repopulations with *Pinus pinaster* Aiton (LPAZ-9). However, the average size of the *Pinus* subgenus *Pinus* pollen in the LPAZ-8 is very similar to that of LPAZ-1 to LPAZ-3, and significantly different to the most modern *Pinus* pollen evidence (LPAZ-9). The average grain size of *Pinus* pollen also decreases in LPAZ-5 and LPAZ-6, which suggests some contributions of reworked ancient *Pinus* to the seabed sediment still took place during the periods of upwelling intensification occurred during the Mid- and Late Holocene (Fig. 9). Nevertheless, the size of those *Pinus* subgenus *Pinus* pollen grains during the Thermal Optimum (LPAZ-4) are like modern pine pollen sizes (LPAZ-9), but significantly different to those recorded in LPAZ-1 to LPAZ-3 and LPAZ-8. Further studies will be necessary to confirm if these trends may be related to the warmer/wetter conditions (Ejsmond et al., 2015; McCulloch et al., 2022) during the Thermal Optimum or if a replacement of pine species (Desprat et al., 2015) took place in the surroundings of RdV between the Lateglacial and the Mid-Holocene.

In relation to the new hornbeam pollen evidence, Muñoz Sobrino et al. (2018) proposed that *Carpinus* survived at the beginning of the Holocene in a variety of habitats in coastal valleys in NW Iberia, which might be comparable to the oak-ash, ravine, and hardwood floodplain forests currently existing in other regions of Europe. Besides, large areas of these coastal ecosystems disappeared when the sea level rose, presumably during the Early Holocene. New multiproxy data presented here reveals (Fig. 5) that *Carpinus* pollen evidence consistently accreted in RdV until ca. 4000 cal a BP, just before the shift towards more oceanic hydrological conditions (Fig. 4) and the re-acceleration of the RSL rise during the second half of the Holocene (García-Artola et al., 2018). A realistic possibility is that this material has been resedimented along the mid-Holocene, together with the reworked *Pinus* pollen. Nevertheless, there is no correlation between the concentrations of *Carpinus* recorded below 75 cm depth in the core and those of *Pinus* subgenus *Pinus* observed at similar depths, perhaps because they do not respond to the same reworking processes (Fig. 10B). Alternatively, a positive low correlation ($r^2 = 0.4$) exists between the concentrations of *Carpinus* and *Quercus robur*-type in the sediment (Fig. 10C), which suggests that hornbeam also persisted until almost the Late Holocene in some coastal environments of NW Iberia as it happened in some upland areas of the region (Muñoz Sobrino et al., 2018).

5.3. Implications for stratigraphic and sedimentary studies

Sediment recycling poses a challenge to the accurate reconstruction of allogenic signals from sedimentary archives, as transfer zones within sedimentary systems act as dynamics areas where sedimentary processes can buffer or mask environmental signals (Romans et al., 2016; Toby et al., 2019; Griffin et al., 2023). The evidence of reworked pollen identified and characterised in RdV offers valuable insights into sedimentary processes during the Holocene transgression in the incised valley. Significant sediment reworking likely takes place during the transgression, particularly associated with transgressive erosive surfaces such as the tidal and wave ravinement (Catuneanu et al., 2011; Zecchin and Catuneanu, 2013).

Lantzsch et al. (2010) argued that sediment recycling played an important role in sediment buildup on the NW Iberian shelf during its deglacial drowning leading to the formation of a gravel-rich lag. Cartelle et al. (2022) reported that tidal ravinement processes were associated with peaks in sediment recycling in another ria system, the Ría de Arousa (Fig. 1A), which is comparable to RdV. Besides, they hypothesised that this process also had a significant impact on the pollen record hindering the identification of oak expansion in the region. The coarse-grain deposits of MVR-3 (Fig. 1B) correspond to high-amplitude reflections in the seismic profiles (Fig. 1C) and display anomalous

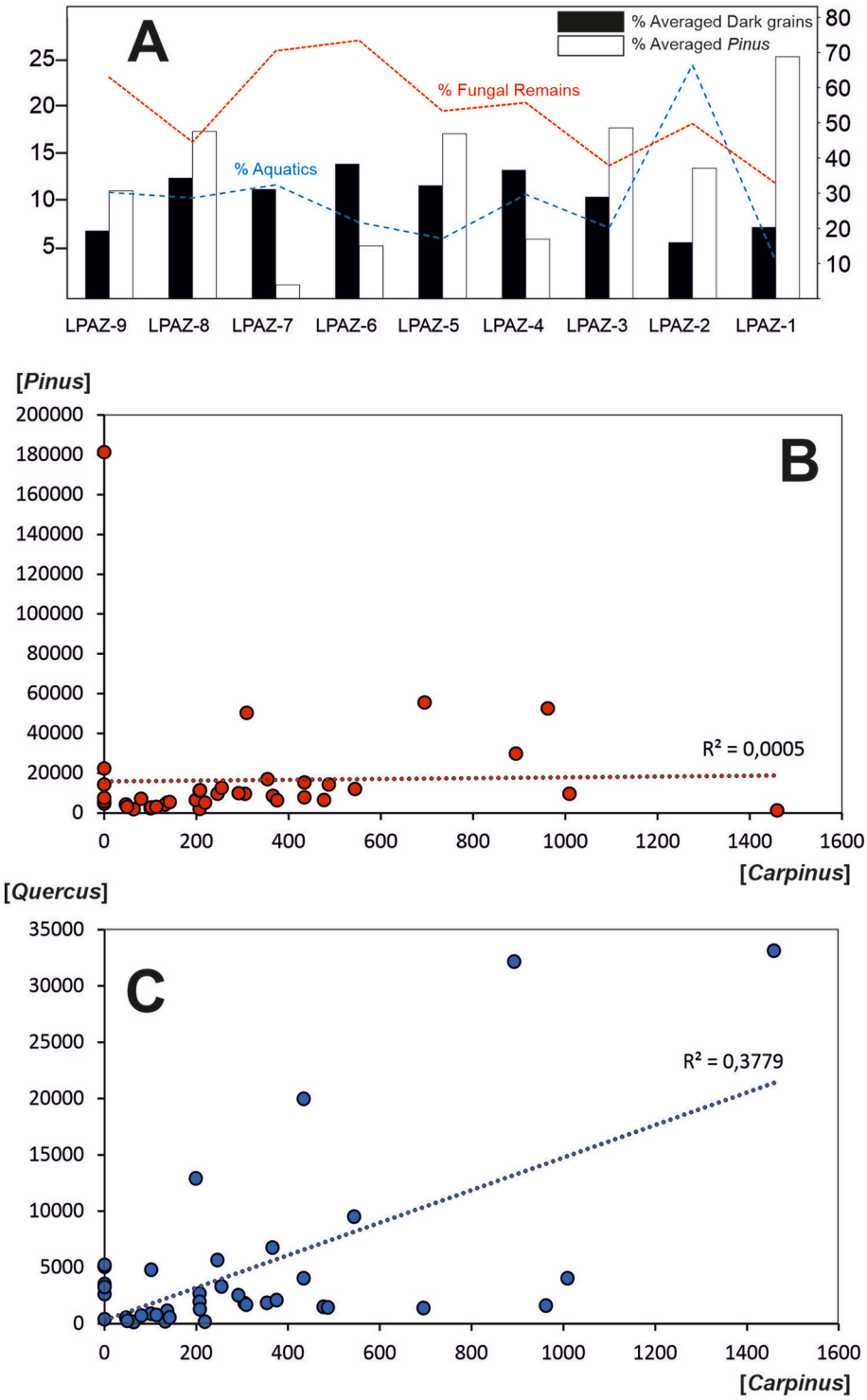

Fig. 10. A) Graphic representation of averaged pollen evidence per LPAZ showed in Table S2; and correlation analyses between *Carpinus*-type pollen concentrations recorded below 75 cm depth in core MVR-3 and concentrations of A) *Pinus* subgenus *Pinus* and B) *Quercus robur*-type at the same levels.

pollen successions rich in pine pollen. These sediments denote erosive surfaces (disconformities) formed within the transgressive deposits; therefore, these are interpreted as transgressive ravinement surfaces. The available multiproxy evidence, combined with RSL reconstructions, support that coastal wetland ecosystems developed onshore in RdV while RSL stayed low (Figs. 8 and 9); and that these ancient sediments might be a realistic primary source for most of those recycled materials identified in seismic units U6 and U7 (Fig. 9).

In RdV, tides and waves are the main drivers of erosion during the transgression, with tidal ravinement usually taking place earlier, during stages of high rates of sea-level rise, and waves becoming dominant after 7-6 ka when the lower rates of sea-level rise allow the waves to erode the margins of the basin effectively (Fig. 9). Both processes are likely contributing to sediment recycling in RdV. However, more detailed stratigraphic analyses are needed to characterise and distinguish both ravinement processes. Nevertheless, the anomalous pollen successions are not only associated with coarse-grained sediments, as these are also found underlying and overlying these ravinement surfaces as part of

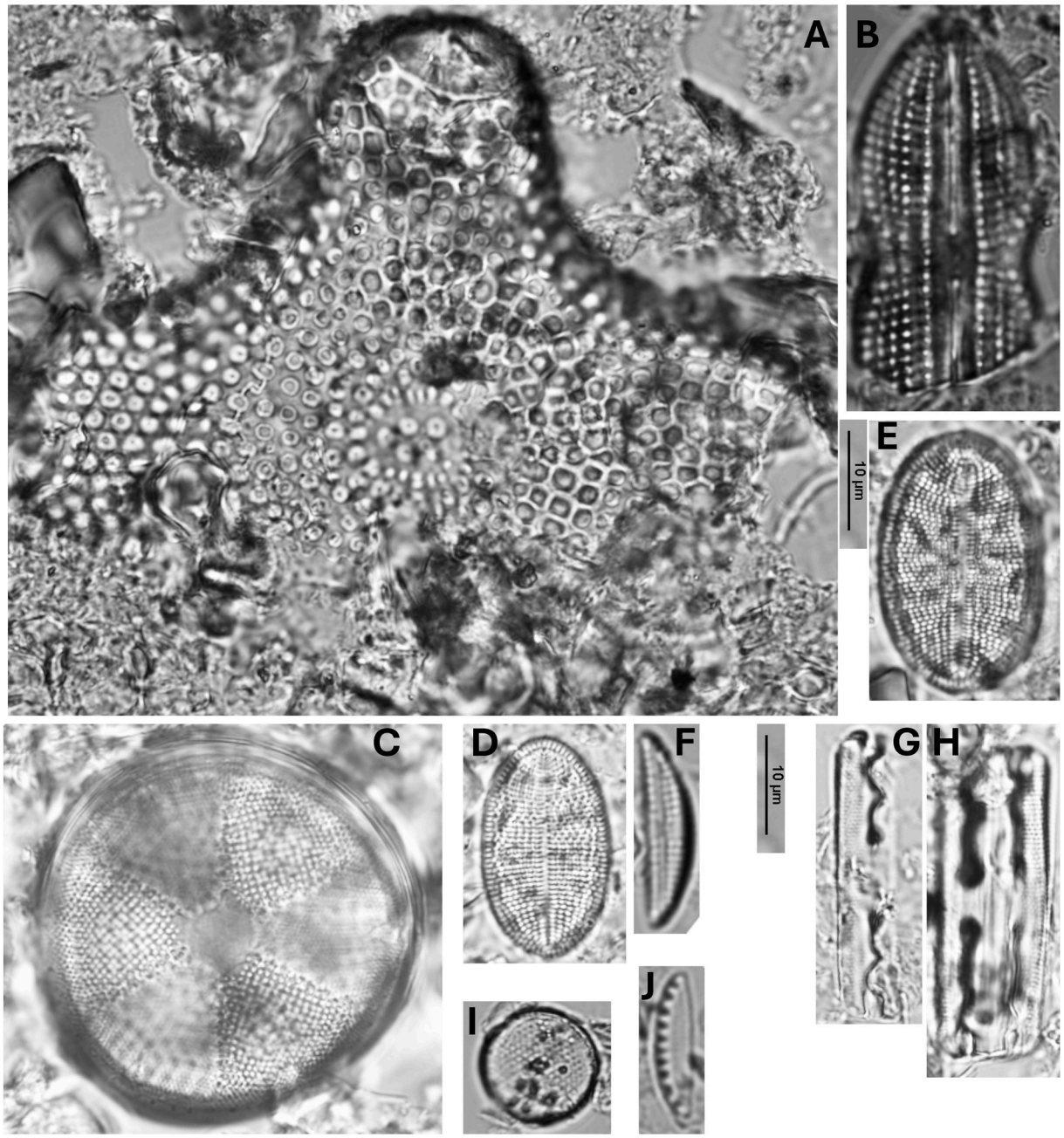

Plate 1. Diatoms. A) *Biddulphia antediluviana*, B) *Diploneis* aff. *stroemii*, C) *Actinoptychus senarius*, D-E) *Cocconeis* aff. *euglypta*, F) *Amphora* aff. *pediculus*, G-H) *Grammatophora* sp., I) *Actinocyclus* sp., J) *Nitzschia* aff. *inconspicua*. Scale Bar 10 µm.

sandy or silty deposits in U6 and U7. This indicates that sediment recycling is widespread and persistent through most of the transgression during the entire Holocene. This sediment recycling is still probably related to the same transgressive erosive processes as the ravinement surfaces, but it is not easily identifiable as there is no clear expression in the seismic or sedimentary datasets.

6. Conclusions

Radiocarbon dates from macroremains (shells) and microremains (extracted pollen) were combined on the studied section of sediment to obtain improved environmental reconstructions. This methodology enables the building of a coherent regional model that explains the reworking of coastal and upland sediments during the marine transgression and their redeposition inside the basin. This new approach serves to refine previous interpretations of the seismic records and improves our understanding of the climatic and environmental dynamics in the Galician *Rías Baixas* during the Holocene, the timing of the regional marine transgression, and their joint impact on the local development of highly sensitive (ephemeral) coastal ecosystems.

Dinoflagellate cyst records in combination with the contemporaneous (not reworked) pollen evidence reveal a reliable climatic seesaw during the Holocene in Ría de Vigo. Periods of prevailing mixed waters (wet stormy periods with strong development of *Lingulodinium* and high accumulation rates in dinoflagellate cyst) alternate with other sparsely stormy and drier phases, characterised by the coastal upwelling intensification and more stratified waters (increasing *Bitectatodinium* and *Spiniferites* spp. but low accumulation rates in dinoflagellate cysts). These climatic dynamics, including a millennial dry cool period that occurred just after the Holocene Climatic Optimum are consistent with

previous evidence obtained in mountain lakes, ombrotrophic peat bogs, and other limnetic systems from NW Iberia, the Duero Depression and Mediterranean mountains systems from Southern Iberia. Furthermore, there is a delay between the two phases with the highest marine contribution to sediment (ca. 11.0-8.2 and ca. 4.0-3.0 ka BP) and the subsequent warm stages when the RSL stabilises: the Climatic Optimum (8.0–6.0 ka BP) and the 2.5-0.5 ka BP interval, respectively.

Besides, differential dating revealed that some levels with anomalous pollen successions are conspicuously aged and have inverted pollen chronologies. These facies may constitute evidence of redeposition of ancient upland sediments, formed above de ancient coastline at different intervals comprised between the end of the last glacial maximum and the early stages of the Lateglacial.

Changes in *Pinus* pollen concentrations and total pollen grain sizes recorded in the postglacial sediments suggest that some upland ancient (Lateglacial) pollen evidence might be remobilised, especially during stages of upwelling intensification, and then resedimented in the seabed. Further studies will be needed to determine if the significant differences existing between the pollen grain sizes respond to climatic variations affecting the region or have been the result of any replacement of pine species in the area: i.e. some temperate species (*P. sylvestris/P. nigra*) being replaced by Mediterranean pines (*P. pinaster/P. pinea/P. halepensis*). In any case, *Pinus* subgenus *Pinus* pollen evidence almost disappeared with the first signs of anthropisation in the area, and only recovered after modern repopulations. Alternatively, the new evidence discussed also supports that hornbeam persisted in the Ría de Vigo basin until ca. 4.0 ka BP.

Our findings in Ría de Vigo open up new possibilities to further our understanding of sediment reworking and recycling mechanisms through the integration of multiproxy studies encompassing pollen, seismic and sedimentary data. This integrated approach broadens our understanding and offers more comprehensive perspectives on the interplay of environmental processes. Moreover, extrapolating our methodology to larger scales may allow to understand the impact of autogenic processes on palaeoenvironmental records across diverse sediment transport systems, including estuaries. Our study underscores these processes in the record of the sediment core MVR-3, which reveals the significant impact of sediment recycling on other proxies and palaeoenvironmental indicators, as the overrepresentation of pine pollen may mask other species that are more significant to understand climate dynamics. This also highlights the need for multiproxy approaches, as misinterpretations may originate from reworked pollen or micropalaeontological remains that were not identified as recycled.

Main authors contributions

Main authors' specific contributions: CMS and ACP, produced the new pollen data and conceived the idea. VC, NMC and SGG produced, elaborated, and interpreted seismic records and geochemical data. CD studied the diatoms content, and NC and IL make the biometric study of pollen grains. All authors contributed to sampling, discussion, and preparation of the manuscript.

Declaration of competing interest

The authors declare that they have no known competing financial interests or personal relationships that could have appeared to influence the work reported in this paper.

Acknowledgements

This work was funded by the Spanish Ministry of Education and Science CGL2012-33584 (co-financed with ERDF funds), Spanish Ministry of Science Innovation and Universities PID2023-147147OB-I00 (co-financed with ERDF funds) and Spanish Ministry of Science and Innovation the European NextGeneration EU Funds TED2021-131141B-I00; the Xunta de Galicia GRC 2015/020 and ED431C 2019/28 projects; and the Axudas Propias a Investigación da Universidade de Vigo 2024.

Appendix A. Supplementary data

Supplementary data to this article can be found online at https://doi.org/10.1016/j.quascirev.2024.109006.

Data availability

Data will be made available on request.

References

Abrantes, F., 1991. Increased upwelling off Portugal during the last glaciation: diatom evidence. Mar. Micropaleontol. 17 (3–4), 285–310.

Barton, E.D., Largier, J.L., Torres, R., Sheridan, M., Trasviña, A., Souza, A., Pazos, Y., Valle-Levinson, A., 2015. Coastal upwelling and downwelling forcing of circulation in a semi-enclosed bay: Ria de Vigo. Prog. Oceanogr. 134, 173–189.

Benito, G., Greenbaum, N., Medialdea, A., Calle, M., Sanchez-Moya, Y., Machado, M., Ballesteros-Cánovas, J., 2023. Late Pleistocene–Holocene multi-decadal patterns of extreme floods in NW Iberia: the Duero River palaeoflood record. Quat. Sci. Rev. 321, 108356. https://doi.org/10.1016/j.quascirev.2023.108356.

Bernal-Wormull, J.L., Moreno, A., Bartolomé, M., Arriolabengoa, M., Pérez-Mejías, C., Iriarte, E., Osácar, C., Spötl, C., Stoll, H., Cacho, I., Edwards, R.L., Cheng, H., 2023. New insights into the climate of northern Iberia during the younger Dryas and Holocene: the mendukilo multi-speleothem record. Quat. Sci. Rev. 305, 108006. https://doi.org/10.1016/j.quascirev.2023.108006.

Blaauw, M., Christen, J.A., 2011. Flexible paleoclimate age-depth models using an autoregressive gamma process. Bayesian Analysis 6 (3), 457–474. https://doi.org/10.1214/11-BA618.

Björk, S., Wohlfarth, B., 2001. ^{14}C chronostratigraphic techniques in paleolimnology. In: Last, W.M., Smol, J.P. (Eds.), Tracking Environmental Change Using Lake Sediments. Volume I: Basin Analysis, Coring, and Chronological Techniques. Kluwer Academic Publishers, Dordrecht, pp. 205–245.

Bond, G., Showers, W., Cheseby, M., Lotti, R., Almasi, P., deMenocal, P., Priore, P., Cullen, H., Hajdas, I., Bonaniet, G., 1997. A pervasive millennial-scale cycle in the North Atlantic Holocene and glacial climates. Science 294, 2130–2136.

Bouhier, A., 2001. Galicia. Ensaio Xeográfico de Análise e Interpretación dun Vello Complexo Agrario. Xunta de Galicia, Santiago de Compostela, pp. 1407–pp.

Bradley, L., Milne, G.A., Horton, B.P., Zong, Y., 2016. Modelling sea level data from China and Malay-Thailand to estimate Holocene ice-volume equivalent sea level change. Quat. Sci. Rev. 137, 54–68.

Brown, T.A., Farwell, G.W., Grootes, P.M., Schmidt, F.H., 1992. Radiocarbon AMS dating of pollen extracted from peat samples. Radiocarbon 34, 550–556.

Cajade-Pascual, D., Costa-Casais, M., Blanco-Chao, R., Taboada Rodríguez, T., 2023. Sea-level change and human occupation over 6000 years on Areoso Island (Ría de Arousa, NW Iberian Peninsula). Environ. Earth Sci. 82, 260. https://doi.org/10.1007/s12665-023-10955-7.

Cartelle, V., García-Gil, S., 2019. From a river valley to a ria: Evolution of an incised valley (Ría de Ferrol, north-west Spain) since the Last Glacial Maximum. Sedimentology 66 (5), 1930–1966, 10.1111/.

Cartelle, V., García-Moreiras, I., Martínez-Carreño, N., Muñoz Sobrino, C., García-Gil, S., 2022. The role of antecedent morphology and changing sediment sources in the postglacial palaeogeographical evolution of an incised valley: the sedimentary record of the Ría de Arousa (NW Iberia). Global Planet. Change 208, 103727. https://doi.org/10.1016/j.gloplacha.2021.103727.

Castro-Parada, A., Muñoz Sobrino, C., 2022. Variations in modern pollen distribution in sediments from nearby upland lakes: implications for the interpretation of paleoecological data. Rev. Palaeobot. Palynol. 306, 104765. https://doi.org/10.1016/j.revpalbo.2022.104765.

Castro-Parada, A., Muñoz Sobrino, C., Ferreiro da Costa, J., Cartelle, V., MartínezCarreño, N., García-Gil, S., 2023. Pollen sedimentation in fluvio-marine systems: a comparison between modern pollen evidence in sea-floor coastal lagoons and upland ponds from Ría de Vigo, NW Iberia. XXI INQUA Congress Roma 13–20. July 2023.

Costas, S., Muñoz Sobrino, C., Alejo, I., Pérez-Arlucea, M., 2009. Holocene evolution of a rock-bounded barrier lagoon system, Cíes Islands, northwest Iberia. Earth Surf. Process. Landf. 34, 1575–1586.

Cushing, E.J., 1964. Redeposited pollen in Late-Wisconsin pollen spectra from East-Central Minnesota. Am. J. Sci. 262, 1075–1088.

Catuneanu, Octavian, Galloway, William E., Kendall, Christopher G.S.t.C., Miall, Andrew D., Posamentier, Henry W., Strasser, André, Tucker, Maurice E., 2011. Sequence stratigraphy: methodology and nomenclature. Newsl. Stratigr. 44 (3), 173–245. https://doi.org/10.1127/0078-0421/2011/0011.

Dai, L., Weng, C., Lu, J., Mao, L., 2014. Pollen quantitative distribution in marine and fluvial surface sediments from the northern South China Sea: new insights into pollen transportation and deposition mechanisms. Quat. Int. 325, 136–149. https://doi.org/10.1016/j.quaint.2013.09.031.

Dias, J.A.M., Boski, T., Rodrigues, A., Magalhaes, F., 2000. Coast line evolution in Portugal since the Last Glacial Maximum until present – a synthesis. Mar. Geol. 170, 177–186.

Desprat, S., Sánchez-Goñi, M.F., Loutre, M.F., 2003. Revealing climatic variability of the last three millennia in northwestern Iberia using pollen influx data. Earth Planet Sci. Lett. 213, 63–78.

Desprat, S., Díaz Fernández, P.M., Coulon, T., Ezzat, L., Pessarossi-Langlois, J., Gil, L., Morales-Molino, C., Sánchez-Goñi, M.F., 2015. *Pinus nigra* (European black pine) as the dominant species of the last glacial pinewoods in south-western to central Iberia: a morphological study of modern and fossil pollen. J. Biogeogr. 42, 1998–2009. http://wileyonlinelibrary.com/journal/jbidoi:10.1111/jbi.12566.

de Vernal, A., 2009. Marine palynology and its use for studying nearshore environments. In: IOP Conference Series: Earth and Environmental Science, vol. 5, 012002. https://doi.org/10.1088/1755-1307/5/1/012002. From Deep-Sea To Coastal Zones: Methods And Techniques For Studying Paleoenvironments, 25–29 February 2008, Faro, Portugal.

Donders, T.H., Van Helmond, N.A., Verreussel, R., Munsterman, D., ten Veen, J., Speijer, R.P., Weijers, J.W., Sangiorgi, F., Peterse, F., Reichart, G.-J., 2018. Land–sea coupling of early Pleistocene glacial cycles in the southern North Sea exhibit dominant Northern Hemisphere forcing. Clim. Past 14, 397–411. https://doi.org/10.5194/cp-14-397-2018.

Ejsmond, M.J., Ejsmond, A., Banaisak, L., Karpinska-Kolaczek, M., Kozlowski, J., Kolazeck, P., 2015. Large pollen at high temperature: an adaptation to increased competition on the stigma? Plant Ecol. 216, 1407–1417. https://doi.org/10.1007/s11258-015-0519-z.

Faegri, K., Iversen, J., Krzywinski, K., 1989. Textbook of Pollen Analysis, fourth ed. John Wiley and Sons Ltd., London, p. 328.

Fernández-López, J., Fernández.Cruz, J., Míguez-Soto, B., 2021. The demographic history of Castanea sativa Mill. in southwestEurope: A natural population structure modified bytranslocations. Molecular Ecology 30, 3930–3947. https://doi.org/10.1111/mec.16013.

Fernández-Salas, L.M., Durán, R., Mendes, I., Galparsoro, I., Lobo, F.J., Bárcenas, P., Rosa, F., Ribó, M., García-Gil, S., Ferrín, A., Carrara, G., Roque, C., Canals, M., 2015. Shelves of the Iberian Peninsula and the Balearic islands (I): Morphology and sediment types. Bol. Geol. Min. 126, 327–376.

Figueroa, R.I., Bravo, I., 2005. Sexual reproduction and two different encystment strategies of Lingulodinium polyedrum (Dinophyceae) in culture. J. Phycol. 41, 370–379.

Fletcher, W.J., Sánchez Goñi, M.F., Naughton, F., Seppä, H., 2024. Chapter 6 – greenlandian stage (early Holocene, 11.7–8.2ka). In: Palacios, D., Hughes, P.D., Jomelli, V., Tanarro, L.M. (Eds.), European Glacial Landscapes. Elsevier, pp. 73–87. https://doi.org/10.1016/B978-0-323-99712-6.00029-5.

García-Artola, A., Stéphan, P., Cearreta, A., Kopp, R.E., Khan, N.S., Horton, B.P., 2018. Holocene sea-level database from the Atlantic coast of Europe. Quat. Sci. Rev. 196, 177–192. https://doi.org/10.1016/j.quascirev.2018.07.031.

García-Moreiras, I., Vila Costas, S., García-Gil, S., Muñoz Sobrino, C., 2023. Organic-walled dinoflagellate cyst assemblages in surface sediments of the Ría de Vigo (Atlantic margin of NW Iberia) in relation to environmental gradients. Mar. Micropaleontol. https://doi.org/10.1016/j.marmicro.2023.102217.

García-Moreiras, I., Cartelle, V., Garcia-Gil, S., Muñoz Sobrino, C., 2019a. First high-resolution multi-proxy palaeoenvironmental record of the Late Glacial to Early Holocene transition in the Ría de Arousa (Atlantic margin of NW Iberia). Quat. Sci. Rev. 215, 308–321. https://doi.org/10.1016/j.quascirev.2019.05.016.

García-Moreiras, I., Delgado, C., Martínez-Carreño, N., Garcia-Gil, S., Muñoz Sobrino, C., 2019b. Climate and vegetation changes in coastal ecosystems during the Middle Pleniglacial and the early Holocene: Two multi-proxy, high-resolution records from Ría de Vigo (NW Iberia). Global Planet. Change 176, 100–122. https://doi.org/10.1016/j.gloplacha.2019.02.015.

García-Moreiras, I., Pospelova, V., García-Gil, S., Muñoz Sobrino, C., 2018. Climatic and anthropogenic impacts on the Ría de Vigo (NW Iberia) over the last two centuries: a high-resolution dinoflagellate cyst sedimentary record. Palaeogeogr. Palaeoclimatol. Palaeoecol. 504, 201–218. https://doi.org/10.1016/j.palaeo.2018.05.032.

García-Moreiras, I., Sánchez, J.M., Muñoz Sobrino, C., 2015. Modern pollen and non-pollen palynomorph assemblages of salt marsh and subtidal environments from the Ría de Vigo (NW Iberia). Rev. Palaeobot. Palynol. 219, 157–171. https://doi.org/10.1016/j.revpalbo.2015.04.006.

Gardoki, J., Cearreta, A., Irabien, M.J., Gómez-Arozamena, J., Villasante-Marcos, V., García-Artola, A., Galaz-Samaniego, C.A., Peñalba, M.C., Bessa, F., 2023. Modern conditions and recent environmental evolution of the industrialized inner Ría of Ferrol (Galicia, NW Spain). Coastal Shelf Research 267, 105098. https://doi.org/10.1016/j.csr.2023.105098.

Gomez-Orellana, L., Ramil-Rego, P., Muñoz Sobrino, C., 1998. Una nueva secuencia polínica y cronológica para el depósito pleistoceno de Mougás (NW de la Península Ibérica). Review of Paléobiolgie 17, 35–47.

Gómez-Orellana, L., Ramil-Rego, P., Ferreiro da Costa, J., Muñoz Sobrino, C., 2021. Holocene environmental change on the Atlantic coast of NW Iberia as inferred from the Ponzos wetland sequence. Boreas 50 (4), 1131–1145, 10.1111/bor.v50.410.1111/bor.12535.

González-Villanueva, R., Pérez-Arlucea, M., Costas, S., Bao, R., Otero, X.L., Goble, R., 2015. 8000 years of environmental evolution of barrier–lagoon systems emplaced in coastal embayments (NW Iberia). The Holocene 25, 1786–1801. https://doi.org/10.1177/0959683615591351.

Goslin, J., Sansjofre, P., Van Vliet-Lanoe, B.V., Denmark, C., 2017. Carbon stable isotope and elemental (TOC, TN) geochemistry in salymarsh surface sediments (western brittany, France): a useful tool for reconstructing Holocene relative seasea-level. J. Quat. Sci. 32 (7), 987–1007. https://doi.org/10.1002/jqs.2971.

Griffin, C., Duller, R.A., Straub, K.M., 2023. The degradation and detection of environmental signals in sediment transport systems. Sci. Adv. 9 (44). https://doi.org/10.1126/sciadv.adi8046.

Grimm, E., 1990-2019. TILIA and TILIA graph: PC spreadsheets and graphics software for pollen data. INQUA commission for the study of the Holocene working group data handling methods. Newsletter 4, 5–7.

Hammer, Ø., Harper, D.A.T., Ryan, P.D., 2001. PAST: paleontological statistics software for education and data analysis. Paleontologia Electronica 4 (1), 9. http://palaeo-electronica.org/2001_1/past/issue1_01.htm.

Hasle, G.R., Syvertsen, E.E., 1996. Marine diatoms. In: Tomas, C.R. (Ed.), Identifying Marine Diatoms and Dinoflagellates. Academic Press, Inc., San Diego, pp. 1–385.

Heiri, H., Brooks, S.J., Renssen, H., Bedford, A., Hazekamp, M., Ilyashuk, B., Jeffers, E.S., Lang, B., Kirilova, E., Kuiper, S., Millet, L., Samartin, S., Toth, M., Verbruggen, F., Watson, J.E., van Asch, N., Lammertsma, E., Amon, L., Birks, H.H., Birks, H.J.B., Mortensen, M.F., Hoek, W.Z., Magyari, E., Muñoz Sobrino, C., Seppa, H., Tinner, W., Tonkov, S., Veski, S., Lotter, A.F., 2014. Validation of climate model-inferred regional temperature change for late-glacial Europe. Nat. Commun. 5, 4914. https://doi.org/10.1038/ncomms5914.

Hopkins, J.A., McCarthy, F.M.G., 2002. Oxidation and the palynological record. Palynology 26, 266–267.

Iriarte-Chiapusso, M.J., Muñoz Sobrino, C., Gomez-Orellana, L., Hernandez-Beloqui, B., García-Moreiras, I., Fernández Rodriguez, C., Heiri, O., Lotter, A.F., Ramil-Rego, P., 2016. Reviewing the Lateglacial/Holocene transition in NW Iberia: A palaeoecological approach based on the comparison between dissimilar regions. Quaternary International 403, 211–236. https://doi.org/10.1016/j.quaint.2015.09.029.

Jiménez-Moreno, G., Heiri, O., García-Alix, A., Anderson, R.S., Jiménez-Espejo, F.J., López-Blanco, C., Jiménez, L., Pérez-Martínez, C., Rodrigo-Gámiz, M., López-Avilés, A., Camuera, J., 2023. Holocene summer temperature reconstruction based on a chironomid record from Sierra Nevada, southern Spain. Quat. Sci. Rev. 319, 108343. https://doi.org/10.1016/j.quascirev.2023.108343.

Justino, F., Peltier, W.R., 2005. The glacial North Atlantic oscillation. Geophys. Res. Lett. 32, L21803. https://doi.org/10.1029/2005GL023822.

Kaal, J., Carrión Marco, Y., Asouti, E., Martín Seijo, M., Martínez Cortizas, A., Costa Casais, M., Criado Boado, F., 2011. Long-term deforestation in NW Spain: linking the Holocene fire history to vegetation change and human activities. Quat. Sci. Rev. 30, 161–175. https://doi.org/10.1016/j.quascirev.2010.10.006.

Keil, R.G., Hu, F.S., Tsamakis, E.C., Hedges, J.I., 2014. Pollen in marine sediments as an indicator of oxidation of organic matter. Nature 369, 639–641.

Krammer, K., Lange-Bertalot, H., 1991. Bacillariophyceae 4. Teil: achnanthaceae. In: Ettl, H., Gärtner, G., Gerloff, J., Heynig, H., Mollenhauer, D. (Eds.), Süßwasserflora von Mitteleuropa, Band 2/4. Gustav Fischer Verlag, Heidelberg, p. 437.

Krammer, K., Lange-Bertalot, H., 1999a. Bacillariophyceae 1. Teil: naviculaceae. In: Ettl, H., Gärtner, G., Gerloff, J., Heynig, H., Mollenhauer, D. (Eds.), Süßwasserflora von Mitteleuropa, Band 2/1. Gustav Fischer Verlag, Heidelberg, p. 876.

Krammer, K., Lange-Bertalot, H., 1999b. Bacillariophyceae 2. Teil: bacillariaceae, epithemiaceae, surirellaceae. In: Ettl, H., Gärtner, G., Gerloff, J., Heynig, H., Mollenhauer, D. (Eds.), Süßwasserflora von Mitteleuropa, Band 2/2. Gustav Fischer Verlag, Heidelberg, p. 611.

Krammer, K., Lange-Bertalot, H., 2000. Bacillariophyceae 3. Teil: centrales, fragilariaceae, eunotiaceae. In: Ettl, H., Gärtner, G., Gerloff, J., Heynig, H., Mollenhauer, D. (Eds.), Süßwasserflora von Mitteleuropa, Band 2/3. Gustav Fischer Verlag, Heidelberg, p. 599.

Krebs, P., Ulmke, F., Tinner, W., Conedera, M., 2022. The Roman Legacy on European Chestnut and Walnut Arboriculture. Environmental Archeology. https://doi.org/10.1080/14614103.2022.2137648.

Krüger, S., Damrath, M., 2020. In search of the Bølling-Oscillation: a new high resolution pollen record from the locus classicus Lake Bølling, Denmark. Veg. Hist. Archaeobotany 29, 189–211. https://doi.org/10.1007/s00334-019-00736-3.

Kvavadze, E.V., 1996. Redeposited pollen in recent and Holocene sediments of the Caucasus mountains. Grana 35 (1), 33–37. https://doi.org/10.1080/00173139609430498.

Lamb, A.L., Wilson, G.P., Leng, M.J., 2006. A review of coastal palaeoclimate and relative sea-level reconstructions using δ13C and C/N ratios in organic material. Earth Sci. Rev. 75, 29–57.

Lange-Bertalot, H., 1993. 85 neue Taxa und über 100 weitere neu definierte Taxa ergänzend zur Süsswasserflora von Mitteleuropa 2/1-4. Biology Diatomology 27, 1–454.

Lange-Bertalot, H., 2001. Navicula sensu stricto. 10 genera separated from Navicula sensu lato. Frustulia. In: Lange-Bertalot, H. (Ed.), Diatoms of Europe, vol. 2, p. 526.

Lantzsch, H., Hanebuth, T.J.J., Henrich, R., 2010. Sediment recycling and adjustment of deposition during deglacial drowning of a low-accumulation shelf (NW Iberia). Continent. Shelf Res. 30, 1665–1679. https://doi.org/10.1016/j.csr.2010.06.013.

Lee, S.A., Kim, T.H., Kim, G., 2020. Tracing terrestrial versus marine sources of dissolved organic carbon in a coastal bay using stable carbon isotopes. Biogeosciences 17, 135–144. https://doi.org/10.5194/bg-17-135-2020.

Leorri, E., Fatela, F., Drago, T., Bradley, S.L., Moreno, J., Cearreta, A., 2013. Lateglacial and Holocene coastal evolution in the Minho estuary (N Portugal): implications for understanding sea-level changes in Atlantic Iberia. Holocene 23 (3), 353–363. https://doi.org/10.1177/0959683612460786.

Levkov, Z., Caput Mihalič, K., Ector, L., 2010. A taxonomical study of Rhoicosphenia Grunow (Bacillariophyceae) with a key for identification of selected taxa. Fottea 10, 145–200.

Li, Y., Wang, N.A., Li, Z.L., Zhang, C.Q., Zhou, X.H., 2012. Reworking effects in the Holocene Zhuye Lake sediments: a case study by pollen concentrates AMS ^{14}C dating. Sci. China Earth Sciencies 55, 1669–1678. https://doi.org/10.1007/s11430-012-4482-4.

López-Merino, L. Tallón-Armada. R., Costa-Casais, M., Silva-Sánchez, N., López-Sáez, J. A., Martínez Cortizas, A., 2023. Palaeoenvironmental Framing of the O Areal Roman Saltworks and Related Anthropogenic Activities in North-western Iberia. Environmental Archaeology. https://doi.org/10.1080/14614103.2023.2206199.

López-Merino, L., Leroy, S.A.G., Eshel, A., Epshtein, V., Belmaker, R., Bookman, B., 2016. Using palynology to re-assess the Dead Sea laminated sediments - indeed varves? Quat. Sci. Rev. 140, 49–66. https://doi.org/10.1016/j.quascirev.2016.03.024.

Lorenzo, M.N., Taboada, J.J., Gimeno, L., 2008. Links between circulation weather types and teleconnection patterns and their influence on precipitation patterns in Galicia (NW Spain). Int. J. Climatol. 28, 1493–1505. https://doi.org/10.1002/joc.1646.

Luo, C., Chen, M., Xiang, R., Liu, J., Zhan, L., Lu, J., Yang, M., 2014. Modern pollen distribution in marine sediments from the northern part of the South China Sea. Mar. Micropaleontol. 108, 41–56. https://doi.org/10.1016/j.marmicro.2014.03.001.

Martínez-Carreño, N., García-Gil, S., 2017. Reinterpretation of the Quaternary sedimentary infill of the Ría de Vigo, NW Iberian Peninsula, as a compound incised valley. Quat. Sci. Rev. 173, 124–144. https://doi.org/10.1016/j.quascirev.2017.08.015.

Martínez-Carreño, N., García-Gil, S., Cartelle, V., 2017. An unusual Holocene fan-shaped subaqueous prograding body at the back of the Cíes Islands ridge (Ría de Vigo, NW Spain): Geomorphology, facies and stratigraphic architecture. Mar. Geol. 385, 13–26.

Matero, I.S.O., Gregoire, L.J., Ivanovic, R.F., Tindall, J.C., Haywood, A.M., 2017. The 8.2 ka cooling event caused by Laurentide ice saddle collapse. Earth Planet Sci. Lett. 473, 205–214.

Max, L., Nürberg, D., Chiessi, C.M., Lenz, M.M., Mulitza, S., 2022. Subsurface ocean warming preceded Heinrich Events. Nat. Commun. 13, 4217. https://doi.org/10.1038/s41467-022-31754-x.

McCarthy, F.M.G., Mudie, P.J., 1998. Oceanic pollen transport and pollen: dinocyst ratios as markers of late Cenozoic sea level change and sediment transport. Palaeogeogr. Palaeoclimatol. Palaeoecol. 138, 187–206.

McCulloch, R.D., Mathiasen, P., Premoli, A., 2022. Palaeoecological evidence of pollen morphological changes: a climate change adaptation strategy? Palaeogeogr. Palaeoclimatol. Palaeoecol. 601, 111157. https://doi.org/10.1016/j.palaeo.2022.111157.

Mertens, K.N., Verhoeven, K., Verleye, T., Louwye, S., Amorim, A., Ribeiro, S., Deaf, A.S., Harding, I.C., De Schepper, S., Gonzalez, C., Kodrans-Nsiah, M., De Vernal, A., Henry, M., Radi, T., Dybkjaer, K., Poulsen, N.E., Feist-Burkhardt, S., Chitolie, J., Heilmann-Clausen, C., Londeix, L., Turon, J.-L., Marret, F., Matthiessen, J., McCarthy, F.M.G., Prasad, V., Pospelova, V., Hughes, J.E.K., Riding, J.B., Rochon, A., Sangiorgi, F., Welters, N., Sinclair, N., Thun, C., Solima, A., Van Nieuwenhove, N., Vink, A., Young, M., 2009. Determining the absolute abundance of dinoflagellate cysts in recent marine sediments: the Lycopodium marker-grain method put to the test. Review of Palaeobotany and. Palynology 157 (3), 238–252.

Morales-Molino, C., García-Antón, M., Postigo-Mijarra, J.M., Morla, C., 2013. Holocene vegetation, fire and climate interactions on the westernmost fringe of the Mediterranean Basin. Quat. Sci. Rev. 59, 5–17. https://doi.org/10.1016/j.quascirev.2012.10.027.

Moore, P.D., Webb, J.A., Collinson, M.E., 1991. Pollen Analysis. Blackwell, London, p. 216.

Moreno, A., Svensson, A, Brooks, S.J., Connor, S., Engels, S., Fletcher, W, Genty, D., Heiri, O., Labuhn, I., Persoui, A., Peyron, O., Valero-Garcés, B., Wulf, S., Zanchetta, G., Allen, J.R.M., Ampel, L., Blamart, D., Birks, H., Blockley, S., Borsato, A., Bos, H., Brauer, A., Combourieu-Nebout, N., de Beaulieu, J.-L., Drescher-Schneider, R., Drysdale, R., Elias, S., Frisia, S., Hellstrom, J., Ilyashuk, B., Joannin, S., Kühl, N., Larocque-Tobler, I., Lotter, A., Magny, M., Matthews, I., McDermott, F., Millet, L., Morellón, M., Neugebauer, I., Muñoz Sobrino, C., Naughton, F., Ohlwein, C., Roucoux, K., Samartin, S., Sánchez-Goñi, M.-F., Sirocko, F., van Asch, N., van Geel, B., van Grafenstein, U., Vannière, B., Vegas, J., Veres, D., Walker, M., Wohlfarth, B., 2014. Compilation of Western European terrestrial records 60-8 ka BP: towards an understanding of latitudinal climatic gradients. Quaternary Science Reviews 106, 167–185. https://doi.org/10.1016/j.quascirev.2014.06.030.

Mudie, P.J., Yanko-Hombach, V.V., Mudryk, I., 2021. Palynomorphs in surface sediments of the North-Western Black Sea as indicators of environmental conditions. Quat. Int. 590, 122–145. https://doi.org/10.1016/j.quaint.2020.05.014.

Muñoz Sobrino, C., Ramil-Rego, P., Rodríguez Guitián, M., 1997. Upland vegetation in the north-west Iberian Peninsula after the last glaciation: forest history and deforestation dynamics. Veg. Hist. Archaeobotany 6, 215–233. https://doi.org/10.1007/BF01370443.

Muñoz Sobrino, C., Ramil-Rego, P., Rodríguez Guitián, M.A., 2001. Vegetation in the mountains of northwest Iberia during the last glacial-interglacial transition. Veg. Hist. Archaeobotany 10, 7–21. https://doi.org/10.1007/PL00013366.

Muñoz Sobrino, C., Ramil-Rego, P., Gómez-Orellana, L., Díaz Varela, R.A., 2005. Palynological data on major Holocene climatic events in NW Iberia. Boreas 34, 381–400.

Muñoz Sobrino, C., García-Gil, S., Diez, J.B., Iglesias, J., 2007. Palynological characterization of gassy sediments in the inner part of Ría de Vigo (NW Spain). New chronological and environmental data. Geo Mar. Lett. 27 (2–4), 289–302.

Muñoz Sobrino, C., Heiri, O., Hazekamp, M., van der Velden, D., Kirilova, E.P., García-Moreiras, I., Lotter, A.F., 2013. New data on the Lateglacial period of SW Europe: a high-resolution multiproxy record from Laguna de la Roya (NW Iberia). Quat. Sci. Rev. 80, 58–77.

Muñoz, Sobrino C., García-Moreiras, I., Castro, Y., Martínez Carreño, N., de Blas, E., Fernandez, Rodríguez C., Judd, A., García-Gil, S., 2014. Climate and anthropogenic factors influencing an estuarine ecosystem from NW Iberia: new high resolution multiproxy analyses from San Simón Bay (Ría de Vigo). Quat. Sci. Rev. 93, 11–33.

Muñoz Sobrino, C., García-Gil, S., Iglesias, J., Martínez Carreño, N., Ferreiro da Costa, J., Díaz Varela, R.A., Judd, A., 2012. Environmental change in the Ría de Vigo, NW Iberia, since the mid-Holocene: new palaeoecological and seismic evidence. Boreas 41, 578–601.

Muñoz Sobrino, C., Cartelle, V., Martínez-Carreño, N., Ramil-Rego, P., García-Gil, S., 2022. The timing of the postglacial marine transgression in the Ría de Ferrol (NW Iberia): a new multiproxy approach from its sedimentary infill. Catena 209, 105847. https://doi.org/10.1016/j.catena.2021.105847.

Muñoz Sobrino, C., García-Moreiras, I., Gómez-Orellana, L., Iriarte-Chiapusso, M.J., Heiri, O., Lotter, A.F., Ramil-Rego, P., 2018. The last hornbeam forests in SW Europe: new evidence on the demise of *Carpinus betulus* in NW Iberia. Vegetation History and Archeobotany 27, 551–576. https://doi.org/10.1007/s00334-017-0654-7.

Muñoz Sobrino, C., García-Moreiras, I., Martínez-Carreño, N., Cartelle, V., Insua, T.L., Ferreiro da Costa, J., Ramil-Rego, P., Fernández Rodríguez, C., Alejo, I., García-Gil, S., 2016. Reconstruction of the environmental history of a coastal insular system using shallow marine records: the last three millennia of the Cíes Islands (Ría de Vigo, NW Iberia). Boreas 45, 729–753. https://doi.org/10.1111/bor.12178.

Nogueira, E., Bravo, I., Montero, P., Díaz-Tapia, P., Calvo, S., Ben-Gigirey, B., Figueroa, R.I., Garrido, J.L., Ramilo, I., Lluch, N., Rossignoli, A.E., Riobó, P., Rodríguez, F., 2022. HABs in coastal upwelling systems: insights from an exceptional red tide of the toxigenic dinoflagellate *Alexandrium minutum*. Ecol. Indicat. 137, 108790. https://doi.org/10.1016/j.ecolind.2022.108790.

Ospina-Alvarez, N., Varela, M., Doval, M.D., Gómez-Gesteira, M., Cervantes-Duarte, R., Prego, R., 2014. Outside the paradigm of upwelling rias in NW Iberian Peninsula: biogeochemical and phytoplankton patterns of a non-upwelling ria. Estuar. Coast Shelf Sci. 138, 1–13.

Otero, P., Ruiz-Villarreal, M., Peliz, A., 2008. Variability of river plumes off Northwest Iberia in response to wind events. J. Mar. Syst. 72, 238–255.

Pena, L.D., Francés, G., Diz, P., Esparza, M., Grimalt, J.O., Nombela, M.A., Alejo, I., 2010. Climate fluctuations during the Holocene in NW Iberia: high and low latitude linkages. Continent. Shelf Res. 30, 1487–1496. https://doi.org/10.1016/j.csr.2010.05.009.

Pérez-Arlucea, M., Álvarez-Iglesias, P., Rubio, B., 2007. Holocene evolution of estuarine and tidal-flat sediments in san Simón bay, Galicia, NW Spain. Journal of Coastal Researh 50, 163–167.

Pérez-Arlucea, M., Filgueira, M., Freijido, M., Mendez, G., 2000. Morphometric and hydrologic parameters of catchments and tributary rivers entering the ria de Vigo. Estimations on annual runoff, suspended and dissolved loads. J. Iber. Geol. 26, 171–187.

Prego, R., Bao, R., Varela, M., Carballeira, R., 2024. Naturally and Anthropogenically Induced Lingulodinium Polyedra Dinoflagellate Red Tides in the Galician Rias (NW Iberian Peninsula. Toxins 16, 280.–toxins16060280.

Ramil Rego, P., Muñoz Sobrino, C., Rodríguez Guitian, M., Gómez Orellana, L., 1998. Differences in the vegetation landscape of the North Iberian Peninsula during the last 16,000 years. Plant Ecology 138, 41–62.

Ramil-Rego, P., Muñoz Sobrino, C., Gómez-Orellana, L., Rodríguez Guitián, M.A., Ferreiro da, Costa. J., 2012. Configuración y transformación del paisaje del NW ibérico durante el final de los tiempos glaciares, el Holoceno y el AntropocenoRecur. Rurais 6, 19–62.

Ramil-Rego, P., Rodríguez Guitián, M.A., Ferreiro Da Costa, J., Rubinos Román, M., Gómez-Orellana, L., de Nóvoa Fernández, B., Hinojo Sánchez, B.A., Martínez Sánchez, S., Cillero Castro, C., Díaz Varela, R.A., Rodríguez González, P.M., Muñoz Sobrino, C., 2008. Os Hábitats de Interese Comunitario en Galicia. Fichas Descritivas. In: Monografías do. Ibader Universidade de Santiago de Compostela, Lugo, p. 627.

Rea, B.R., Pellitero, R., Spagnolo, M., Hughes, P., Ivy-Ochs, S., Renssen, H., Ribolini, A., Bakke, J., Lukas, S., Braithwaite, R.J., 2020. Atmospheric circulation over Europe during the younger Dryas. Sci. Adv. 6, eaba4844.

Rego, P., 2022. Nitrogen fluxes and budget seasonality in the ria Vigo (NW iberian Peninsula). Hydrobiologia 475/476, 161–171.

Reimer, P.J., Reimer, R.W., 2001. A marine reservoir correction database and on-line interface. Radiocarbon 43, 461–463.

Rodríguez, F., Escalera, L., Reguera, B., Nogueira, E., Bode, A., Ruiz-Villareal, M., Rossignoli, A.E., Ben-Gigirey, B., Rey, V., Fraga, S., 2023. Red tides in the Galician rías: historical overview, ecological impact, and future monitoring strategies. Environmental Science Processes & Impacts. https://doi.org/10.1039/d3em00296a.

Romans, B.W., Castelltort, S., Covault, J.A., Fildani, A., Walsh, J.P., 2016. Environmental signal propagation in sedimentary systems across timescales. Earth Sci. Rev. 153, 7–29. https://doi.org/10.1016/j.earscirev.2015.07.012.

Round, F.E., Crawford, D.M., Mann, D.G., 1990. The Diatoms: Biology and Morphology of the Genera. Cambridge University Press, Cambridge, pp. 760–pp.

Sáez, A., Carballeira, R., Pueyo, J.J., Vázquez-Loureiro, D., Leira, M., Hernández, A., Valero-Garcés, B., Bao, R., 2018. Formation and evolution of back-barrier perched lakes in rocky coasts: an example of a Holocene system in north-west Spain. Sedimentology 65, 1891–1917. https://doi.org/10.1111/sed.12451.

Sánchez-Goñi, M.F., Desprat, S., Fletcher, W.J., Morales-Molino, C., Naughton, F., Oliveira, D., Urrego, D.H., Zorzi, C., 2018. Pollen from the deep-sea: a breakthrough in the mystery of the ice ages. Frontiers in Plant Sciences 9, 38. https://doi.org/10.3389/fpls.2018.00038.

Stancliffe, R.P.W., 2002. Microforaminiferal linings. In: Jasionius, J., McGregor, D.C. (Eds.), Palynology: Principles and Applications 1. American Association of Stratigraphical Palynologists Foundation, Dallas, TX, pp. 373–379.

Stanley, E.A., 1966. The problem of reworked pollen and spores in marine sediments. Mar. Geol. 4, 397–408.

Streel, M., Bless, M.J.M., 1980. Ocurrence and significance of reworked palynomorphs. Meded. Rijks Geol. Dienst 32–10, 69–80.
Strother, S.L., Salzmann, U., Sangiorgi, F., Bijl, P.K., Pross, J., Escutia, C., Salabarnada, A., Pound, M.J., Voss, J., Woodward, J., 2017. A new quantitative approach to identify reworking in Eocene to Miocene pollen records from offshore Antarctica using red fluorescence and digital imaging. Biogeosciences 14, 2089–2100. https://doi.org/10.5194/bg-14-2089-2017.
Stuiver, M., Reimer, P.J., Reimer, R.W., 2020. Calib 8.2 [WWW program] at. http://calib.org. (Accessed 5 November 2020).
Toby, S.C., Duller, R.A., De Angelis, S., Straub, K.M., 2019. A stratigraphic framework for the preservation and shredding of environmental signals. Geophys. Res. Lett. 46, 5837–5845. https://doi.org/10.1029/2019GL082555.
Traverse, A., 2008. Paleopalynology, second ed. Springer, Dordrecht, The Nethelands, p. 813. ISBN 978-1-4020-5609-3.
Trobajo, R., Rovira, L., Ector, L., Wetzel, C.E., Kelly, M., Mann, D.G., 2013. Morphology and identity of some ecologically important small Nitzschia species. Diatom Res. 28 (1), 37–59.
Tunno, I., Zimmerman, S.R.H., Brown, T.A., Hassel, C.A., 2021. An improved method for extracting, sorting, and AMS dating of pollen concentrates from lake sediment. Frontiers in Ecological Evolution 9, 668676. https://doi.org/10.3389/fevo.2021.668676.
van der Horst, A., Tinner, W., Ezquerra, F.J., Gobet, E., Lotter, A.F., Morellón, M., Muñoz Sobrino, C., Niffenegger, C., Schwörer, C., Szidat, S., Morales-Molino, C., 2024. Late-glacial and Holocene shifts in the mountain landscapes of the Cantabrian range (northern Spain) in response to changing climate, fire occurrence and land use. Quat. Sci. Rev. 342, 108899. https://doi.org/10.1016/j.quascirev.2024.108899.
van Geel, B., 2003. Non pollen palynomorphs. In: Smol, J.P., Birks, H.J.B., Last, W.M. (Eds.), Tracking Environmental Change Using Lake Sediments 3, Terrestrial, Algal and Siliceous Indicators. Kluwer Academic, Dordrecht, pp. 99–120.
van Geel, B., Coope, G.R., van der Hammen, T., 1989. Palaeoecology and stratigraphy of the Lateglacial type section at Usselo (The Netherlands). Review of Paleobotany and Palynology 60, 25–129.
Villacieros-Robineau, N., Herrera, J.L., Castro, C.G., Piedracoba, S., Roson, G., 2013. Hydrodynamic characterization of the bottom boundary layer in a coastal upwelling system (Ría de Vigo, NW Spain). Continent. Shelf Res. 68, 67–79.
Vázquez Marinelly, C., Moreira Pumar, J., Rodal González, M., 2007. Historia de CangasDeputación de Pontevedra, p. 645.
Wanner, H., Mercolli, L., Grosjean, M., Ritz, S.P., 2015. Holocene climate variability and change; a data-based review. J. Geol. Soc. 172, 254–263. https://doi.org/10.1144/jgs2013e101.
Witkowski, A., Lange-Bertalot, H., Metzeltin, D., 2000. Diatom Flora of Marine Coasts I. Koeltz Scientific Books, Königstein.
Xia, J., Han, Y., Tan, J., Abarike, G.A., Song, Z., 2022. The characteristics of organic carbon in the offshore sediments surrounding the leizhou Peninsula, China. Frontiers Earth Sciencies 10, 648337. https://doi.org/10.3389/feart.2022.648337.
Yedema, Y.W., Donders, T., Peterse, F., Sangiorgi, F., 2023. Dinoflagellate cyst and pollen assemblages as tracers for marine productivity and river input in the northern Gulf of Mexico. J. Micropalaeontology 42, 257–276. https://doi.org/10.5194/jm-42-257-2023.
Yule, B., Roberts, S., Marshall, J.E.A., Milton, J.A., 1998. Quantitative spore colour measurement using colour image analysis. Org. Geochem. 28, 139–149.
Zecchin, M., Catuneanu, O., 2013. High-resolution sequence stratigraphy of clastic shelves I: units and bounding surfaces. Mar. Petrol. Geol. 39 (1), 1–25. https://doi.org/10.1016/j.marpetgeo.2012.08.015.
Zonneveld, Karin A.F., Marret, Fabienne, Versteegh, Gerard J.M., Bogus, Kara, Bonnet, Sophie, Bouimetarhan, Ilham, Crouch, Erica, de Vernal, Anne, Elshanawany, Rehab, Edwards, Lucy, Esper, Oliver, Forke, Sven, Grøsfjeld, Kari, Henry, Maryse, Holzwarth, Ulrike, Kielt, Jean-François, Kim, So-Young, Ladouceur, Sťephanie, Ledu, David, Chen, Liang, Limoges, Audrey, Londeix, Laurent, Lu, S.-H., Mahmoud, Magdy S., Marino, Gianluca, Matsouka, Kazumi, Matthiessen, Jens, Mildenhal, D.C., Mudie, Peta, Neil, H.L., Pospelova, Vera, Qi, Yuzao, Radi, Taoufik, Richerol, Thomas, Rochon, Andŕe, Sangiorgi, Francesca, Solignac, Sandrine, Turon, Jean-Louis, Verleye, Thomas, Wang, Yan, Wang, Zhaohui, Young, Marty, 2013. Atlas of modern dinoflagellate cyst distribution based on 2405 datapoints. Rev. Palaeobot. Palyn. 191, 1–197.